A QUASI ONE-DIMENSIONAL METHOD AND RESULTS FOR STEADY ANNULAR/STRATIFIED SHEAR AND GRAVITY DRIVEN CONDENSING FLOWS

S. Mitra, A. Narain, R. Naik, and S. D. Kulkarni

Department of Mechanical Engineering-Engineering Mechanics
Michigan Technological University
Houghton, MI 49931

ABSTRACT

This paper presents an effective quasi one-dimensional (1-D) computational simulation methodology and some important results for steady annular/stratified (or film wise) internal condensing flows of pure vapor. Though the approach is strictly valid for smooth, laminar vapor/laminar condensate flows, it is also approximately valid for laminar condensate and turbulent vapor which are laminar in the near interface region. In-channel and in-tube flows are considered for a range of gravity component values (from 0g to 1g) in the direction of the flow. The 1-D solutions significantly expedite the process of obtaining full two dimensional (2-D) steady/unsteady computational solutions for these flows. For these flows, three sets of results are presented that are consistent with each other and are obtained from: (i) a full 2-D computational fluid dynamics (CFD) based approach, (ii) quasi-1D approach introduced here, and (iii) relevant experimental results involving partially and fully condensing gravity driven flows of FC-72 vapor. The 1-D approach has been implemented for two types of thermal boundary conditions – viz. specifications of temperature or heat flux profiles for the condensing surface. Besides demonstrating and discussing the differences between shear and gravity driven annular flows, the paper also presents a map that distinguishes shear driven, gravity driven, and "mixed" driven flows within the non-dimensional parameter space for these duct flows. With the help of a proper synthesis with reliable experiments, some useful heat transfer correlations are also presented. The paper also demonstrates that μm-scale hydraulic diameter ducts typically experience shear driven flows and provides some important results/discussions for attaining and maintaining annular/stratified flows under these more challenging conditions.

NOMENCLATURE

C_{p1}	Specific heat of the liquid condensate, J/(kg-K)
D	Inner diameter of tubular test-section, m
Fr_x	Froude number U^2/g_xL_c
Fr_y	Froude number U^2/g_yL_c
h	Channel gap, m
Ja	Condensate liquid Jakob number, $C_{p1} \cdot \Delta T / h_{fg}(p_{in})$
k_1	Conductivity of condensate liquid, W/(m-K)
L	Length of the test-section, m
L_C	Characteristic length, L_C = D (diameter) for tubes and L_C = h (gap height) for channels, m
$\dot{M}_{in}$	Vapor flow rate at test-section inlet, g/s or kg/s
$\dot{M}_L$	Liquid flow rate at test-section exit, g/s or kg/s
p_{in}	Pressure at the test-section inlet, kPa
p_{exit}	Pressure at the test-section exit, kPa
Pr_1	Condensate liquid Prandtl number, $\mu_1 \cdot C_{p1} / k_1$
$\dot{Q}_{total}$	Net heat rate out of the test-section, W
Re_{in}	Inlet vapor Reynolds number, $\rho_2 U L_c/\mu_2$
t	Non-dimensional time
t	Physical time, s
θ	Non-dimensional temperature
$T_{sat}(p)$	Saturation temperature at pressure p, ^oC
$\overline{T}_w$	Mean condensing surface temperature, ^oC
U	Average inlet vapor velocity in the x-direction, m/s
u_f	Non-dimensional interfacial velocity in the x-direction
u_1	Physical velocity in the x-direction, m/s
v_1	Physical velocity in the y-direction, m/s
v	Non-dimensional velocity in the y-direction
x, y	Physical distances along and perpendicular to the condensing surface, m

x, y	Non-dimensional distances along and perpendicular to the condensing surface
x_{FC}	Approximate length needed for full condensation (estimted by computations), m.
x_{FC}	Non-dimensional x_{FC}.
ΔT	$T_{sat}(p) - \overline{T}_w$, ^oC
Δp	$p_{in} - p_{exit}$, kPa
Δ	Physical value of condensate thickness, m
δ	Non-dimensional value of condensate thickness
ρ_2	Density of vapor, kg/m^3
ρ_1	Density of liquid, kg/m^3
μ_2	Viscosity of vapor, kg/(m-s)
μ_1	Viscosity of liquid, kg/(m-s)
π_e	Non-dimensional exit pressure
ζ	Non-dimensional pressure gradient $d\pi/dx$

Subscripts

comp	Obtained from computations
E	Test-section exit
Expt	Obtained from experiments
I	I = 1 for liquid and I = 2 for vapor
in	Test-section inlet
Na	Natural exit condition
Nu	Nusselt solution
ps	Pure shear case

1. INTRODUCTION

Reliable design and effective integration of condensers in traditional macro-scale as well as modern micro-scale thermal systems require good flow prediction capabilities and proper flow control strategies. For this, one needs to investigate issues pertaining to attainability of steady/quasi-steady flows in different flow regimes. Among these regimes, particular interest is

in attainability and controllability of annular/stratified (or film wise condensation) flows under gravity or shear driven conditions. This is because annular/stratified flows have high thermal efficiencies and should be rigorously studied (i.e. by a synthesis of computations and experiments) to: (i) develop predictive abilities, and (ii) develop the boundaries between annular stratified and adjacent flow regimes (such as plug/slug, bubbly, etc. discussed in [1]) in the context of the general non-dimensional parameter space considered here. However, this paper addresses only the first of these two objectives.

For shear or gravity driven annular/stratified internal partially condensing flows (as in the channel of Fig. 1a or vertical tube of Fig. 1b) with a given inlet vapor mass flow rate and a known vapor to wall temperature difference, our earlier established computational and experimental results (Narain et. al. [2] - [7]) have been corrected (also see Narain et. al. [8] - [10]) to state that there exists a *unique* annular/stratified steady solution and a unique steady exit condition of the strictly steady equations. The multiple steady solutions that were reported to exist in [2]-[7] were not *all* strictly steady solutions (see [10]). In fact all but one of them were quasi-steady (steady-in-the-mean) solutions [10] mistaken for strictly steady solutions. Here and henceforth, the unique steady solutions for the steady "parabolic" boundary conditions, namely, the *inlet* conditions (vapor mass flow rate, pressure, and temperature) and thermal boundary condition for the condensing-surface (i.e. known uniform or non-uniform spatial variations for the condensing surface's temperature or heat-flux values) are termed "natural" solutions. The value of an appropriate exit parameter (exit pressure, or exit liquid mass flow rate, or exit vapor mass flow rate) obtained from the "natural" solution is termed "natural" exit condition for the flow.

The new "quasi" 1-D technique presented and implemented here is different from the other 1-D tools ([11], [12], [13], etc.) that are available in the literature. This 1-D tool avoids the use of average flow variables and/or empirical models (such as friction factor models for the interface, pressure gradient models, etc) used in [11] – [13] by keeping the method close to the exact solution technique for laminar vapor and laminar liquid flows (with smooth or nearly smooth wavy interface). Because of the absence of empirical/semi-empirical models in the formulation, the results from this computationally efficient 1-D technique are shown to be in agreement with the results obtained from a full 2-D CFD technique as well as numerous relevant experimental runs ([9], [14], and [15]) for which the modeling assumptions of this paper hold.

The paper presents key differences between purely shear driven and gravity dominated (and driven) annular flows inside tubes and channels. A map that partitions the parameter space (for annular/stratified flows) into strongly gravity driven, shear driven, and "mixed" driven regions is presented here. The solutions of the unsteady governing equations in the vicinity of the steady solutions – both for gravity dominated and shear dominated flow zone are important in understanding various issues of the flows' sensitivities to noise and fluctuations at the condenser's boundary (see [10]). The steady results presented here facilitate such investigation. For example, in [10], theory and experiments show that different quasi-steady impositions of pressure–difference affect the solutions for the shear driven cases and result in different quasi-steady annular/stratified flows with different heat transfer rates. Shear driven cases occur in horizontal channels, 0g and - as shown here - in μm scale ducts of any orientation.

If the shear driven case represents a fully condensing flow situation, as the vapor slows down, the resulting steady/unsteady morphology is often more complex (e.g., annular, plug/slug, bubbly, etc. as reported in [10], [16] - [19]). Though annular as well as more complex morphology flows are seen for condensing flows inside a *horizontal* tube ([16]), these flows are quite different from the ones studied here because of their three dimensional nature associated with the presence of azimuthal component of gravity. Inside horizontal tubes, annular flows typically occur for high inlet vapor speeds and more complex flow morphologies occur for slow inlet vapor speeds (see [16]). Unlike this horizontal tube situation, for the gravity driven flows studied here, most flows are annular almost up to the point of full condensation (see [9]). Complex morphologies for gravity driven flows may occur at distances where 70-100% of the incoming vapor flow has already condensed. Also, unlike horizontal tube situation, annular shear driven flows may occur even at smaller vapor flow rates provided the exit condition of the condenser is handled sensitively (e.g., in [10] where the shear driven flows are allowed to self seek their exit condition). However because of the sensitivity of shear driven flows to the nature of exit conditions (see [10]), there are many shear driven situations (see Cheng et. al. [17] – [18], Garimella et. al. [19], etc.) where annular flows may not occur.

This paper, however, limits itself to the theory and results demonstrating the efficacy of the 1-D method for finding steady annular/stratified "natural" solutions under steady "parabolic" boundary conditions. The methodology presented here has an ability to find "natural" solutions for uniform or non-uniform prescriptions for temperature or heat flux boundary conditions for

the condensing-surface. This capability is very useful in solving conjugate heat transfer problems involving condensers.

The paper also shows how condensing flows inside straight ducts of μm-scale hydraulic diameter allow purely shear driven flows regardless of the duct's orientation with respect to the gravity vector.

2. COMPUTATIONAL APPROACH

This paper presents a unique and new implementation of a one-dimensional (1-D) approach towards meaningful and useful synthesis with a full two-dimensional (2-D) computational approach for solving steady and unsteady equations that model steady annular/stratified (or film wise) internal condensing flow problems. The governing equations for 1-D steady and 2-D steady/unsteady approaches are described here. Both the solution techniques focus on channel and tube flow situations involving laminar condensate and laminar vapor (vapor flow needs to be laminar only in the "near-interface" region). The thermal boundary condition for the condensing-surface, in the one-dimensional approach, allows imposition of either a known temperature or a known heat flux variation.

The liquid and vapor phases in the flows of interest (see Figs. 1a – 1b) are denoted by $\mathcal{L}$ (I = 1) for liquid and $\mathcal{V}$ (I = 2) for vapor. The fluid properties (density ρ, viscosity μ, specific heat C_p, and thermal conductivity k) with subscript I are assumed to take their representative constant values for each phase (I = 1 or 2). Let T_I be the temperature fields, p_I be the pressure fields, T_{sat} (p) be the saturation temperature of the vapor as a function of local pressure p, Δ be the film thickness, $\dot{m}$ be the local interfacial mass flux, T_w (x) (< T_{sat} (p)) be a known temperature variation of the condensing surface, and $\mathbf{v}_I = u_I\hat{\mathbf{i}}+v_I\hat{\mathbf{j}}$ be the velocity fields. Furthermore, the characteristic length L_c for the channel geometry is its channel gap 'h' shown in Fig. 1a and, for the tube geometry, L_c is the diameter D shown in Fig. 1b. Let g_x and g_y be the components of gravity along x and y axes, $p_{in} \equiv p_0$ be the inlet pressure, $\Delta T(x) \equiv T_{sat}(p_{in}) - T_w(x)$ be a representative controlling temperature difference between the vapor and the bottom plate, $\Delta T \equiv T_{sat}(p_{in}) - \overline{T}_W$ be a reference temperature difference (where $\overline{T}_W$ is the mean condenser surface temperature), h_{fg} be the heat of vaporization at local saturation temperature T_{sat} (p)

associated with local interfacial pressure p, and U be the average inlet vapor speed determined by the inlet mass flux. Let t represent the actual time and (x, y) represent the physical distances of a point with respect to the axes shown in Figs. 1a – 1b (x = 0 is at the inlet, y = 0 is at the condensing surface). For the tube flow in Fig. 1b, the (x, r) axes are related to the (x, y) axes through y = D/2 – r. For the channel of height (or channel gap) 'h', y = h is an isothermal slightly superheated non-condensing surface and, for the tube, y = D/2 (i.e. r = 0) is the center-line where symmetry condition holds for all flow variables of interest. Note that for both channel flow (Fig. 1a) and in-tube (Fig. 1b) flows, $y \equiv L_c.y$ represents the distance from the condenser surface. We introduce a list of fundamental non-dimensional variables – viz. $(x, y, t, \delta, u_I, v_I, \pi_I, \theta_I, \dot{m})$ through the following definitions:

$$\{x, y, \Delta, u_I, \dot{m}\} \equiv \{L_C \cdot x, L_C \cdot y, L_C \cdot \delta, U \cdot u_I, \rho_I \cdot U \cdot \dot{m}\}$$
$$\{v_I, T_I, p_I, t\} \equiv \{U \cdot v_I, (\Delta T) \cdot \theta_I, p_0 + \rho_I U^2 \cdot \pi_I, (L_C / U) \cdot t\}. \quad (1)$$

Two-dimensional (2-D) Approach:

The governing non-dimensional differential forms of mass, momentum (x and y components), and energy equations for incompressible flow in the interior of either of the phases, the interface conditions, inlet conditions, and the wall conditions have been given and discussed in detail in other papers ([3], [5] - [7]) and are not reported here for brevity.

A detailed description of the 2-D steady/unsteady computational approach utilized in this paper is given in section 3 of Narain et al. [5]. A brief description of all essential features of computational approach is also available in section 3 of Liang et al. [4] and in Kulkarni et al. [10].

Quasi One Dimensional (1-D) Approach:

The steady solutions for shear and gravity driven flows in Figs. 1a – 1b that have been obtained by a 2-D approach for the steady 2-D equations cited above, can also be obtained by a computationally more efficient and versatile (i.e. over a larger parameter zone), though more approximate, 1-D solution technique that is reported here. This is an important tool that has been developed as an independent tool as well as a tool that supports and improves the efficacy of the

associated 2-D approaches. The 1-D technique is different from most other 1-D tools ([11], [12], and [13]) that use average flow variables and incorporate assumed empirical models (such as friction factor models for the interface, pressure gradient models, certain turbulence models, etc.) in the solution procedure. For laminar vapor and thin laminar condensate flows, the method reported here is called "quasi" 1-D because it is analytically exact except for an approximated assumption on the nature of the cross-sectional variation (i.e. y-variation) of the vapor profile $u_2(x,y)$. In the 1-D solution technique such as this, integral forms of vapor phase momentum and mass balances are used to minimize the impact, that arise from the assumed nature of y-variation of the vapor velocity profile, on the predicted values of the one-dimensional variables of interest.

The differential form of the governing equations for laminar condensate (I = 1) flows (x and y components of the momentum balance and the energy equation) are simplified under the assumptions of steady flows, boundary layer approximations ($\partial/\partial x \ll \partial/\partial y$ & $v_I \ll u_I$), negligible inertia in the momentum equations, and negligible convection terms in the energy equation. These simplified equations are:

$$0 \cong u_1 \frac{\partial u_1}{\partial x} + v_1 \frac{\partial v_1}{\partial x} \cong \frac{1}{Re_1} \frac{\partial^2 u_1}{\partial x^2} - \frac{\partial \pi_1}{\partial x} + Fr_x^{-1}$$

$$-\frac{\partial \pi_1}{\partial y} + Fr_y^{-1} \cong 0, \text{ and}$$

$$0 \cong \frac{1}{Re_I Pr_I}\left(\frac{\partial^2 \theta_I}{\partial y^2}\right) \tag{2}$$

In Eq. (2) above, $Re_I \equiv (\rho_I\, U\, L_c)/\mu_I$, $Fr^{-1}_x \equiv g_x\, L_c/\, U^2$, $Fr^{-1}_y \equiv g_y\, L_c\, /\, U^2$, and $Pr_I \equiv \mu_I\, C_{pI}/k_I$. In addition to the approximation leading to Eq. (2), this formulation also assumes uniform cross-sectional pressure assumption for the vapor phase ($p_2 = p_2(x) = p_0 + \rho_2 U^2 \pi_2(x)$ with $\pi \equiv \pi_2\,(x)$ and $\pi(0) = 0$), negligible impact of vapor super heat, and negligible interfacial slope approximation $\left(\delta'(x)^2 \ll 1\right)$. As a result, interface conditions given by Eqs. (3) - (9) of [5] are simplified and replaced by Eqs. (3) - (6) given below:

$$u_2^i = u_1^i = u_f(x) \tag{3}$$

$$\pi_1^i = \frac{\rho_2}{\rho_1}\pi_2^i = \frac{\rho_2}{\rho_1}\pi(x) \tag{4}$$

$$\left.\frac{\partial u_1}{\partial y}\right|^{i} = \frac{\mu_2}{\mu_1}\left.\frac{\partial u_2}{\partial y}\right|^{i} \tag{5}$$

$$\dot{m}_{Energy} \cong Ja/(Re_1 Pr_1)\left\{\partial\theta_1/\partial y|^{i}\right\} \tag{6}$$

In Eq. (6) above, $Ja \equiv C_{pl}\,\Delta T/h_{fg}(p_0)$. A characteristic length, $L_c = h$ (for the channel case) and $L_c = D$ (for the tube case) is chosen to define the inlet Reynolds number $Re_{in} = \rho_2 U L_c/\mu_2$. The non-dimensional variable definitions introduced in Eq. (1) remains valid for both channel and tube geometries. For thin condensate motion ($\delta \ll 1$, etc), the inertia term in the first equality in Eq. (2) is dropped for I = 1 as this does not alter the solution of the original problem for the range of parameters and flow conditions of interest here. The validity of this modeling approximation is verified through comparison of solutions obtained from this approach with those obtained from computationally solving the full equations (which retains liquid inertia terms) in the two-dimensional approach ([10]). These approximations yield an analytical solution (and representation) for the liquid velocity $u_1(x, y)$ and the temperature $\theta_1(x, y)$. These are given as:

$$u_1(x,y) = \left\{-\frac{d\pi(x)}{dx} + \frac{\rho_1}{\rho_2}Fr_x^{-1} - \frac{\rho_1}{\rho_2}Fr_y^{-1}\frac{d\delta}{dx}\right\}\frac{Re_{in}}{2}.\frac{\mu_2}{\mu_1}y(\delta(x) - y) + \frac{u_f(x)}{\delta(x)}y \tag{7}$$

$$\theta_1(x,y) = \varphi_t(x)\frac{y}{\delta(x)} + \theta_W(x) \tag{8}$$

where $\varphi_t(x) \equiv \frac{T_{sat}(p_0)-T_w(x)}{T_{sat}(p_0)-\overline{T}_W} = \frac{\Delta T(x)}{\Delta T}$ and $\theta_W(x) = \frac{T_W(x)}{\Delta T}$. For the case of uniform condensing surface temperature $T_W(x) = \overline{T}_W$ at all x, $\varphi_t(x) = 1$ and $\theta_W(x)$ is a constant equal to $\overline{T}_W/\Delta T$.

The unknown functions appearing in (7) and (8) are: $\delta(x)$, $u_f(x)$, $\pi(x)$, and $\zeta(x) \equiv d\pi(x)/dx$. The equations controlling these variables are: integral forms of mass and momentum balance for the control volume of width 'Δx' (see Fig. 1a) and the interface conditions in Eqs. (3) - (6). The integral mass and momentum balance equations for the vapor phase motion at any x in the channel geometry are respectively given as:

$$\dot{m}(x) = \frac{d}{dx}\left\{\int_0^{\delta(x)} u_1(x,y)dy\right\} = -\frac{\rho_2}{\rho_1}\left\{\frac{d}{dx}\int_{\delta(x)}^{1} u_2(x,y)dy\right\} \tag{9}$$

and

$$-\frac{d\pi(x)}{dx}\{1-\delta(x)\}+\frac{1}{Re_{in}}\left[\frac{\partial u_2(x,1)}{\partial y}-\frac{\partial u_2\big(x,\delta(x)\big)}{\partial y}\right]-\frac{\rho_1}{\rho_2}\dot{m}(x)u_f(x)\ +\ Fr_x^{-1}\{1-\delta(x)\}$$

$$=\frac{d}{dx}\left[\int_{\delta(x)}^{1}u_2{}^2(x,y)dy\right]. \tag{10}$$

For the in-tube geometry, corresponding equations at any x in the tube, under the notation $\hat{r}\equiv r/D$, are given as:

$$\dot{m}(x)=\frac{2}{1-2\delta}\frac{d}{dx}\left\{\int_{\frac{1-2\delta}{2}}^{\frac{1}{2}}u_1(x,\hat{r})\,\hat{r}.d\hat{r}\right\}=-\frac{2}{1-2\delta}\frac{\rho_2}{\rho_1}\frac{d}{dx}\left\{\int_0^{\frac{1-2\delta}{2}}u_2\hat{r}\,.d\hat{r}\right\} \tag{11}$$

and

$$-\frac{d\pi(x)}{dx}\left\{\frac{(1-2\delta)^2}{8}\right\}+Fr_x^{-1}\frac{(1-2\delta)^2}{8}-\frac{1}{2}\frac{\mu_1}{\mu_2}.\frac{1}{Re_{in}}\frac{\partial u_1}{\partial y}\bigg|^{i}(1-2\delta)$$

$$=\frac{d}{dx}\left\{\int_0^{\frac{1-2\delta}{2}}u_2{}^2\hat{r}\,.d\hat{r}\right\}+\frac{1}{2}\frac{\rho_1}{\rho_2}(1-2\delta)\dot{m}(x)u_f(x). \tag{12}$$

For the in-channel geometry, the equations (5), (6), (9), and (10) are to be satisfied for a reasonable choice for the vapor velocity profile $u_2(x, y)$. One such reasonable choice used in this paper is:

$$u_2(x,y)=\ u_f\frac{1-y}{1-\delta}+b_1(x)\left[\frac{y-\delta}{1-\delta}\left\{\frac{y-\delta}{1-\delta}-1\right\}\right] \tag{13}$$

In Eq. (13), the requirement of onset of condensation at x = 0 demands $\delta(0) = 0$, and $u_f(0) = 0$. The requirement that the inlet vapor velocity profile $u_2 = U.u_2(0,y)$ be a fully developed parabola with an average speed of U demands that $b_1(0) = 6$.

To get an additional estimate for validation and regularity of this 1-D approach, another choice for $u_2(x,y)$ that was used is:

$$u_2(x,y)=b_2(x)\{(y-\delta)-(y-\delta)^2\}+u_f(x)\left[1-(y-\delta)\left\{\frac{6\delta}{u_f}+\frac{1}{1-\delta}\right\}\right] \tag{14}$$

In Eq. (14), the requirements of onset of condensation at x = 0 and a fully developed parabolic velocity profile $u_2 = U.u_2(0,y)$ at the inlet, yields: $\delta(0) = 0$, $u_f(0) = 0$ and $b_2(0) = 6$.

The choices in Eq. (13) or Eq. (14) are consistent with the liquid velocity profile representation in Eq. (7). Therefore these choices automatically satisfy Eq. (3).

For the vertical in-tube case of Fig. 1b, the expected symmetry of the vapor velocity makes a good choice for vapor velocity easier and more accurate than the asymmetric channel case considered here. The good choice employed in this paper is:

$$u_2(x,\hat{r}) = 4\,\frac{u_f(x)-u_m(x)}{(1-2\delta)^2}\hat{r}^2 + u_m(x) \tag{15}$$

In Eq. (15), the requirements of the onset of condensation and a fully developed parabolic velocity profile $\mathcal{U}_2 = U.u_2(0,r)$ at the inlet yields: $\delta(0) = 0$, $u_f(0) = 0$, and $u_m(0) = 2$.

The use of interface shear condition in Eq. (5), effectively expresses the unknown functions - $b_1(x)$ in Eq. (13) or $b_2(x)$ in Eq. (14) or $u_m(x)$ in Eq. (15) – in terms of the primary unknown functions: $\delta(x)$, $u_f(x)$, $\pi(x)$, and $\zeta(x) \equiv d\pi(x)/dx$.

<u>Formulation for known condensing surface temperature boundary condition of $T_l(x,0) = T_w(x)$</u>

With the algebra done on a suitable symbolic manipulation software (e.g. Mathematica from Wolfram Research Inc., USA), the formulation for both the in-tube and in-channel laminar/laminar steady annular/stratified flows (for 1g or 0g) are obtained from the defining equation $d\pi(x)/dx \equiv \zeta(x)$, and three independent governing equations arising from: interface energy balance in Eq. (6), integral mass balance in Eq. (9) or Eq. (11), and integral vapor momentum balance in Eq. (10) or Eq. (12). These governing equations are obtained after substituting for u_1 from Eq. (7), θ_1 from Eq. (8), and u_2 from Eq. (13) or Eq. (14) or Eq. (15) as the case may be. These four governing equations are written in the following vector form of a coupled set of four first order non-linear ordinary differential equations:

$$\mathbf{A}\frac{dy}{dx} = \mathbf{f}(\mathbf{y},x) \tag{16}$$

$$\mathbf{y}(x) \equiv [u_f(x),\ \delta(x),\ \pi(x),\ \zeta(x)]^T$$

$$\mathbf{A} = \begin{bmatrix} 0 & 0 & 1 & 0 \\ A_{11} & A_{12} & 0 & A_{14} \\ C_{11} & C_{12} & C_{13} & C_{14} \\ D_{11} & D_{12} & 0 & D_{14} \end{bmatrix}$$

$$\mathbf{f}(\mathbf{y}, x) = [\zeta(x), 0, f_3, f_4]$$

with known non-linear functions (of **y** and x) for A_{11}, A_{12}, A_{14}, C_{11}, C_{12}, C_{13}, C_{14}, D_{11}, D_{12}, D_{14}, f_3 and f_4 (obtained from symbolic manipulation software). These functions are not reported here for brevity (however their computer generated forms are available).

The problem in Eq. (16) is equivalently posed as:

$$\frac{d\mathbf{y}}{dx} \equiv \mathbf{A}^{-1}.\ \mathbf{f}(\mathbf{y}, x) \equiv \mathbf{g}(\mathbf{y}, x) \tag{17}$$

where, at x = 0, we have the requirements

$$\mathbf{y}(0) = [0, 0, 0, \zeta(0^+)]^{\,T} \tag{18}$$

In the formulation in Eq. (17), the function $\mathbf{g}(\mathbf{y}, x)$ explicitly depends on x only for a known non-uniform prescription for the condensing surface temperature $T_w(x)$. The function $\mathbf{g}(\mathbf{y}, x) = \mathbf{g}(\mathbf{y})$ is independent of x for the uniform prescription of condensing surface temperature $T_w(x) = \overline{T}_w$ for all x. Unless otherwise stated, the thermal boundary condition is always assumed to be one of uniform condensing surface temperature $\overline{T}_w$.

The solutions of the integral formulation (17) - (18) have not been previously implemented in the known literature. This is partly because both $\zeta(0^+)$ in $\mathbf{y}(0)$ in Eq. (18) and $\mathbf{g}(\mathbf{y}(0),0)$ in Eq. (17) are not defined as they are unbounded in the limit of $x \rightarrow 0$. This makes the non-linear ODE problem "singular" and outside the realm of validity of the typical existence/uniqueness theorem for ODEs (see [20]-[21]). Therefore, one has the following possibilities: a unique solution exists, no solution exists, or multiple solutions exist.

It should also be noted that the presence of $d^2\pi/dx^2 = d\zeta/dx$ terms in the formulation of Eq. (17) makes the formulation different from strictly "parabolic" formulations for single-phase and air-water duct flows (where $\dot{m} = 0$) because formulations for such flows only exhibit presence of the first order $d\pi/dx$ terms (not $d^2\pi/dx^2$). Such strictly parabolic forms would only involve a vector of the type $\mathbf{y}(x) \equiv [u_f(x), \delta(x), \pi(x)]^T$ with well defined $\mathbf{y}(0)$. The steady formulation in Eq. (18) is not "elliptic" either because it is computationally found that one does not have multiple solutions with different approaches to $\zeta(0^+)$ that are associated with distinctly different exit pressures $\pi(x_e)$ at $x = x_e$. However the unsteady governing equations associated with the

steady problem in Eqs. (17) – (18) show elliptic dependence on exit boundary conditions (see [10]) and perhaps this is the reason for the unusual appearance of $d^2\pi/dx^2$ terms in the lower order formulation in Eqs. (17) – (18).

Fortunately, despite the singularity at x=0, Eqs. (17) - (18) are integrable. The solution for $x \geq \varepsilon$ is obtained by choosing sufficiently small near zero values of $x = \varepsilon$, $u_f(\varepsilon)$, $\delta(\varepsilon)$, $\pi(\varepsilon)$ and obtaining the value of a consistent $\zeta(\varepsilon)$ from the integrated version of the mass balance (integral of Eq. (9) for channel flows and the integral of Eq. (11) for in-tube flows). For example, the integral of Eq. (9) is $\int_0^\delta u_1(x,y)dy + \frac{\rho_2}{\rho_1}\int_\delta^1 u_2(x,y)dy = \frac{\rho_2}{\rho_1}$ and this equation yields $\zeta(\varepsilon)$ in terms of ε, $u_f(\varepsilon)$, $\delta(\varepsilon)$, and $\pi(\varepsilon)$. With this information on $\zeta(\varepsilon)$ available, the problem given by Eqs. (17) – (18) is rewritten, for $x \geq \varepsilon$, as:

$$\frac{dy}{dx} \equiv \mathbf{g}(\mathbf{y}, x) \tag{19}$$

$$\mathbf{y}(\varepsilon) \equiv [u_f(\varepsilon), \delta(\varepsilon), \pi(\varepsilon) \text{and } \zeta(\varepsilon)]^T \tag{20}$$

Equations (19) and (20) are not singular and are solved by one of the several Runge-Kutta solution schemes (e. g. there are several options available on MATLAB from The MathWorks, Inc., MA).

In this paper, we have extensively investigated the solutions of Eqs. (19) – (20) for several channel heights, tube diameters, inlet vapor speeds, condensing surface temperatures, and fluids.

One of the key results established by the unique solution of the singular Eqs. (17) - (18) or its equivalent Eqs. (19) – (20) is that, the steady annular/stratified (or film wise) condensation solution does not "require" prescription of the exit pressure condition on $\pi(x)$ (at some non-zero $x = x_e$) despite the appearance of $d^2\pi/dx^2$ terms in Eq. (17) or Eq. (19). It is clear from the solution that, for existence of a steady annular/stratified partially condensing flow (under shear driven or gravity driven), there exists a unique self-sought value of steady exit pressure (or quality). The unsteady solutions from the full 2-D technique [10] and experimental realizations (see [9]) show that these natural "annular/stratified" steady flows are quite often stable up to certain distances. However, if the flows are shear driven, the corresponding unsteady equations are "elliptic" and the above annular steady solution can only be realized over lengths of the duct

where this solution is stable and, provided, other "non-natural" time varying or steady-in-the-mean exit conditions (e.g. exit pressure) are not externally imposed – in place of the self-sought "natural" exit condition - at the exit of the condenser (see [10]).

For the in-tube flow in Fig. 1b, this solution technique allows an investigation (see subsequent sections) of the role of the gravitational acceleration component g_x on the nature of the flows and how the non-dimensional solution space $\{x, Re_{in}, Ja/Pr_1, G_P = Fr_x^{-1}.Re_{in}^2, Fr_y^{-1}=0, \rho_2/\rho_1, \mu_2/\mu_1\}$ can be divided in a domain where $g_x = 0$ and the flow is purely shear driven and a domain where g_x is sufficiently large and the flow is gravity dominated in the sense that the interface location and the condensate motion is entirely determined by gravity.

For the gravity dominated condensate flows, the gravitational force and wall shear effects are so large relative to interfacial shear effects that gravity fully determines the condensate flow and the interface location. This interface location and associated interfacial mass-flux values then determine the rest of the vapor flow features (such as pressure variations, etc.) in a way that the pre-determined interface location and the condensate motion associated with the interface location remains independent of the inlet vapor mass flow rate.

<u>Formulation for a known condensing surface heat flux ($q''_w(x)$) boundary condition</u>

For condensers operating at known heat flux values $q''_w(x)$ (uniform or non-uniform with distance x) for the condensing surface, the interface energy balance condition in Eq. (6) is no longer considered a governing equation for the unknowns $\{\delta(x), u_f(x), \pi(x), \text{and } \zeta(x)\}$. The heat flux across the condensing-surface ($q''_w(x)$) is nearly equal to the interfacial heat flux ($\dot{m}(x)h_{fg}$) because of the linearity of the temperature profile assumption in Eq. (8) implies straight conductive heat transfer to the condensing-surface. Therefore, using the non-dimensional form of $\dot{m}$ in Eq. (1) and the result for θ_1 in Eq. (8), the interface energy balance in Eq. (6) becomes

$$\frac{q''_w(x)}{\rho_1 U h_{fg}} \cong \dot{m}_{Energy}(x) = \frac{Ja}{Re_1 Pr_1}.\frac{\varphi_t(x)}{\delta(x)} \tag{21}$$

For a known $q''_w(x)$), the equality between the first and the last term in Eq. (21) is treated as an algebraic relation for obtaining $\varphi_t(x)$ (or $T_w(x) = T_{sat}(p_0) - \Delta T.\varphi_t(x)$) once film-thickness $\delta(x)$ has been obtained from the solution procedure described below.

With $\dot{m} = \dot{m}_{Energy}$ becoming a known function through the first equality in Eq. (21), the integral mass balance in Eq. (9) splits into the following two separate equations:

$$\frac{d}{dx}\int_0^{\delta} u_1(x,y)dy = \frac{q''_w(x)}{\rho_1 U h_{fg}}, \qquad \text{and} \tag{22}$$

$$-\frac{\rho_2}{\rho_1}\frac{d}{dx}\int_{\delta}^{1} u_2(x,y)dy = \frac{q''_w(x)}{\rho_1 U h_{fg}}\,. \tag{23}$$

Again, with algebra done with the help of a computer software, the two separate mass balance equations (arising from Eq. (9) or Eq. (11)), the vapor momentum balance (from Eq. (10) or Eq. (12)), and the defining equation $d\pi(x)/dx \equiv \zeta(x)$ yield four separate ordinary differential equations (ODEs) and lead to a formulation of the type given in Eq. (17) – (18) or Eq. (19) - (20). The resulting problems is again solved by one of the several Runge-Kutta solution schemes and, after the solutions are obtained, the condensing surface temperature is obtained from Eq. (21) – i.e. through: $T_w(x) = T_{sat}(p_0) - \Delta T\cdot \phi_t(x)$.

For many conjugate problems, however, one may only know (or have an estimate of) heat-flux variations $q''_w(x)$ for a given length of the condenser. But this is different than the ability to "fix" a certain heat flux variation $q''_w(x)$ over the length of a condenser - which is experimentally feasible but is rare in practice. It can be shown that, with regard to the shear driven flows' "elliptic – sensitivity" discussed in [10], the ability to "fix" $q''_w(x)$ over a given length of the condenser not only leads to a known condensing surface temperature $T_w(x)$ but, also, leads to a fixing of the exit–condition's mean value (mean exit pressure or exit quality). This heat-flux "fixing" eliminates some of the shear driven flow's sensitivity to inadvertent time variations in the exit condition (see [10]).

3. COMPUTATIONAL VALIDATION OF THE 1-D RESULTS BY ITS COMPARISON WITH THE 2-D RESULTS

Accuracy of 2-D Approach:

For a computational solution to be accurate, it needs to satisfy the following criteria: (i) the convergence criteria in the interior of each fluid (since finite volume SIMPLER technique is used, it means smallness of "b" defined on p.125 of Patankar [22]), (ii) satisfaction of all the interface conditions, (iii) grid independence of solutions for grids that are sufficiently refined, and (iv) unsteady simulation results for the sensitive interface locations should be free of computational noise in the absence of physical noise. For details, we refer the reader to [4] and [10].

Accuracy of 1-D Approach:

The convergence, grid independence, and accuracy of the ODE solver are well known as a well tested Runge-Kutta solver (MATLAB from The MathWorks, Inc., MA) was used. For representative cases chosen for both gravity and shear driven flows, agreements between the 1-D steady solution and the corresponding 2-D steady solution's film thickness predictions are demonstrated in Figs. 2a–2c. The agreements are good. Similar agreement for other flow variables exists, but is not shown here for brevity. Fig. 2a shows film thickness comparison between 1-D solution and 2-D solution for a flow of R113 in a vertical channel, whereas, Fig. 2b shows, for the flow of R113 vapor, the film thickness comparison for a shear driven flow in a channel in zero gravity. For a gravity driven flow of FC-72 in a vertical tube, Figure 2c compares the flow's solution as obtained by a 2-D and the reported 1-D technique. Because of the superior symmetric vapor velocity profile choices (see Eq. (15) that are possible for zero gravity flow in a tube, 1-D solutions yield even better agreement with the nearly exact 2-D techniques than do the asymmetric vapor velocity profile choices for zero-gravity or horizontal channel flow cases (as in Fig. 2b).

Since this "quasi" 1-D simulation technique is computationally more efficient, it can simulate the flow up to or very near (depending on the underlying issues of flow physics) the point of full condensation with greater ease and lower computational costs. Thus, from here and henceforth in

this paper we will be reporting results from the above introduced (sec - 2), and validated (sec – 3), 1-D approach.

4. APPROXIMATE EQUIVALENCE OF FLOWS IN THE CHANNEL AND THE TUBE GEOMETRIES

Though the in-tube geometry and channel geometry are different for both gravity driven (g_x = 9.8 m/s^2) and shear driven (g_x = 0) cases, one asks, what must be the relationship between the tube diameter 'D' and the channel gap 'h' for the two solutions to be nearly the same with respect to the heat transfer rates (i.e $\delta(x)$). For two flows in these two geometries involving flow of same fluid, at the same inlet pressure $p_{in,}$ the same uniform condensing surface temperature $\overline{T}_{w,}$ and the same average inlet speed U; the flows are governed by the same condensate velocity and temperature profiles given by Eq. (7) - (8) under the non-dimensional numbers {x, Re_{in}, Fr_x^{-1}, Ja/Pr_1, ρ_2/ρ_1, μ_2/μ_1}. These non-dimensional numbers will be identical for

$$L_c = D = h. \tag{24}$$

The agreement under Eq.(24), for gravity driven flows, in the solutions obtained for the different sets of equations for the two geometries are shown in Fig. 3. We generalize this agreement in Fig. 3 to say that if δ_{cyl} and $u_{f\text{-}cyl}$ denotes the soultion for tube geometry and δ_{ch} and $u_{f\text{-}ch}$ denotes the solution for channel geometry - then for D = h, identical fluids, and identical values of p_{in}, U, g_x and ΔT – one finds:

$$\delta_{cyl} \approx \delta_{ch}\ ,\ u_{f\text{-}cyl} \approx u_{f\text{-}ch} \tag{25}$$

at any $x_{cyl} \approx x_{ch}$.

This approximate agreement between the results for the cylinder and channel geometeries is seen only for film thickness ($\delta(x)$), and interfacial speed ($u_f(x)$). However, the mass condensed for the cylinder as compared to the channel, is higher (and x_{FC} for cylinder is smaller) for the same values of p_{in}, U, g_x and ΔT. This is because of the difference in the non-condensing surface areas that the two vapor flows are exposed to and this affects the pressure gradient ($d\pi/dx$) and the rate at which vapor mass flow is condensed.

Also note that the transverse component of gravity vector g_y is zero in the vertical tube case shown in Fig. 1b but is non-zero for inclined or horizontal channel configuration for the flow in Fig. 1a. Therefore, the aforementioned similarity of the tube and channel geometry results as characterized by Eqs. (24) - (25) are good only as long as the transverse component of gravity has no significant role. This is usually true for the inclined channel flows ($g_x \neq 0$), but it fails to be the case for flow in a horizontal channel ($g_x = 0$). This is because of the fact that, since g_x (or G_p) is equal to zero for both horizontal and 0g channel cases, the momentum of the liquid condensate is relatively weak and this makes the presence (as in the horizontal channel) or absence (as in 0g) of transverse gravity play an important role – typically after a certain downstream distance when the film is "sufficiently" thick. The result of the role of the transverse gravity is not within the scope of this paper and will be reported elsewhere.

5. COMPUTATIONAL RESULTS ON THE TRANSITION BETWEEN ENTIRELY GRAVITY AND ENTIRELY SHEAR/PRESSURE DRIVEN ANNULAR/STRATIFIED CONDENSING FLOWS

Figure 4a shows the film thickness and cross sectional velocity and temperature profiles for gravity driven ($g_x = 9.8 m/s^2$) and shear driven ($g_x = 0$) condensing flows in a tube under identical flow conditions. It can be seen from Fig. 4a that if all else remains the same, entirely shear driven annular flows have much thicker condensate ($\delta(x) \equiv \delta_{ps}(x)$, where subscript "ps" denotes pure shear) and, hence, much lower heat transfer rates (which is typically inversely proportional to film thickness). The comparative 1-D computational results shown in Figs. 4a–4b for in-tube condensing flows of FC-72 vapor indicate remarkable differences between gravity and shear driven flows with regard to the velocity profiles (see Fig. 4a) and pressure variations (see Fig. 4b).

The velocity profile for gravity driven flow is parabolic in shape with nearly zero slope at the interface (as interfacial shear is not needed to drive the condensate) while the one for shear driven flow is linear with adequate non-zero interfacial shear. For a cooling method that results in only moderate imposition of wall heat-flux, the pressure difference for gravity driven flow often amounts to a pressure rise (see Fig. 4b) as opposed to small pressure drops associated with shear driven 0g flows (also see Fig. 4b). It should be noted that the actual pressure difference in

the vapor phase needs to account for two competing effects: (i) a pressure rise needed for vapor deceleration associated with the size of mass transfer rate across the interface, and (ii) a pressure drop needed to overcome interfacial shear. For the gravity driven flow case in Fig. 4b, it is the vapor deceleration effect that dominates as interfacial shear is allowed to be negligible and for the shear driven case in Fig. 4b, it is the interfacial shear effect that slightly exceeds the vapor deceleration effects (as interfacial mass transfer or wall heat-flux is not too high). For both gravity and shear driven flow cases, however, over the lengths considered, temperature profiles remain linear (see Fig. 4a) even in a full 2-D steady simulation approach.

However, the above comparisons of strictly steady flows are not enough to fully understand the differences between shear driven and gravity driven flows. The reader is referred to [9] and [10] where theory and experimental results show that, compared to gravity driven flows, shear driven unsteady or steady-in-the-mean (quasi-steady) flows show significantly greater sensitivity to: (i) imposition of time varying or quasi-steady pressure-differences through concurrent inlet and exit pressure impositions even as the quasi-steady mass-flow rate through the condenser is held fixed, (ii) noise and vibrations of the condensing surface, and (iii) time-periodic persistent fluctuations in the parabolic boundary conditions of the inlet mass flow rate, inlet pressure, and condensing-surface's thermal conditions.

Gravity driven and shear driven condensing flows inside a channel also show flow features that are very similar to the ones depicted for the in-tube flows (Figs. 4a - 4b), hence these channel flow results are not shown or discussed here for brevity.

At a fixed location $x = x^{\#}$ of an in-tube flow, Fig. 5 shows the variation of film thickness ratio ($\delta(x^{\#})/\delta_{ps}(x^{\#})$) for a flow of FC-72 vapor, as a function of the gravity parameter G_p ($\equiv Fr^{-1}_x * Re_{in}^2 \equiv (\rho_2^2 g_x D_h^3) / \mu_2^2$) when this parameter is increased by changing the gravitational component g_x from $g_x = 0$ to $g_x = 9.81$ m/s^2. Here, $\delta_{ps}(x^{\#})$ is the non-dimensional film thickness at $x = x^{\#}$ for the pure shear case where $G_p = 0$ (i.e. $g_x = 0$). The film thickness ratio $\delta(x^{\#})/\delta_{ps}(x^{\#})$ is equal to 1 for $G_p = 0$ (as $\delta(x) = \delta_{ps}(x)$, for $G_p = 0$), whereas, for $G_p > G_p^*$, the film thickness ratio quickly settles at a number equal to $\delta_{Nu}(x^{\#})/\delta_{ps}(x^{\#})$. Here, $\delta_{Nu}(x)$ is the non-dimensional film thickness for the gravity dominated case given by Eq (10.21) of [23]. For sufficiently large G_p one is in the *gravity dominated* zone for most $x > 0$, and the solution behaves as if $\delta(x) \approx \delta_{Nu}(x)$, where $\delta_{Nu}(x)$ is the classical Nusselt result given by:

$$\delta_{Nu}(x) = \frac{1}{L_c} \bullet [\frac{4 \cdot k_1 \cdot \mu_1 \cdot \Delta T \cdot x}{g \cdot \rho_1 \cdot (\rho_1 - \rho_2) \cdot h_{fg}}]^{1/4}$$

$$\cong [4 \bullet (Ja/Pr_l) \bullet (x/G_p) \bullet (\mu_1/\mu_2)^2 \bullet (\rho_1/\rho_2)^2]^{1/4} \qquad (26)$$

Figure 5 illustrates the significant transitions that take place as G_p increases and that purely shear driven flows seem to exist only for very small near zero G_p values. This discussion emphasizes the need to develop a transition map to demarcate the boundaries between a gravity dominated zone and a purely shear driven zone.

The gravity and shear driven condensing flows for the in-tube flows under varying values of g_x are governed by the following non-dimensional parameters:

$$\{x, Re_{in}, G_p, \frac{\rho_2}{\rho_1}, \frac{\mu_2}{\mu_1}, Ja/Pr_l\}, \qquad (27)$$

where $Re_{in} \equiv \rho_2 UD/\mu_2$, $G_p \equiv Fr^{-1}_x * Re_{in}^2 \equiv \rho_2^2.g_x.D_h^3 / \mu_2^2$, and $Ja/Pr_1 \equiv \Delta T.k_1/h_{fg}.\mu_1$.

Figure 6a shows a division of $\{x, Re_{in}, G_p\}$ space, between gravity dominated and shear driven flows for a given set of values for $\{Ja/Pr_1, \rho_2/\rho_1, \mu_2/\mu_1\}$. To the left of the surface $\sum_1$, the solutions are within 4% of pure shear (g = 0) solution $\delta_{ps}(x)$ and to the right of the surface $\sum_2$, one is within 4% of the gravity dominated Nusselt result $\delta_{Nu}(x)$ given in Eq. (26).

Since all the flow variables (non-dimensional film thickness δ, non-dimensional pressure π, etc.) are functions of the variables listed in Eq. (27), for the purpose of limiting our discussions to some refrigerants (water, FC-72, R-113, etc.) and some commonly occurring situations (U = 0.5 m/s to 3 m/s, D = 1 mm to 7 mm, ΔT = 3 ºC to 25 ºC, etc.), we limit the non-dimensional parameters in Eq. (27) to:

$$0 \le x \le x_A < x_{FC} \quad \text{or} \quad 0 \le x \le x_{0.75} \approx x_A$$

$$900 \le Re_{in} \le 22000$$

$$0.0036 \le Ja/Pr_1 \le 0.0212$$

$$3.2E\text{-}4 \le \rho_2/\rho_1 \le 0.03 \qquad (28)$$

$$0.0113 \le \mu_2/\mu_1 \le 0.06$$

$$57000 \leq G_p \leq 4{,}840{,}000.$$

In the first inequality in Eq. (28), x_A is the approximate length up to which steady annular/stratified flows might actually exist in reality (i.e. the flow is stable and is allowed to self-seek its natural exit condition) and x_{FC} is the length of full condensation. For gravity dominated cases, it is found, both computationally and experimentally [9], that $x_{FC} \approx x_{1.0}$ is the location where approximately 100% of the incoming vapor flow rate is condensed and the flow is still mostly in the wavy annular regime. As a result, the reported 1-D annular flow results are meaningful up to x_{FC} or quite close to it. However, for pure shear driven cases where the flow is allowed to self-seek its natural exit condition, the assumption of annular/stratified flows beyond a certain distance x_A (where A is the number denoting the fraction of $\dot{M}_{in}$ that has condensed up to that location) is generally not true (see [10]) as more complex flow morphologies (such as plug/slug, bubbly, etc. flows) typically occur over a significant distance between x_A and x_{FC}.

It is computationally found that, for the parameter range in Eq. (28), one can solve the steady equations for both gravity and shear driven flows for $0 \leq x \leq x_{0.75}$ where, $x_{0.75}$ ($\equiv x_{0.75}$ (Re_{in}, Ja/Pr_1, G_p, ρ_2/ρ_1, μ_2/μ_1)) is defined to be the distance at which 75% of the incoming vapor flow rate $\dot{M}_{in}$ is condensed.

Furthermore, because condensate flows are thin, it is assumed that the flow conditions are such that the condensate is laminar up to x_{FC} for most cases of interest. This laminar flow assumption is subsequently verified through the well known ([23]) thumb rule which states that, the film Reynolds number $Re_\delta \cong 4\dot{M}_L(x)/\pi D \mu_l$ (where $\dot{M}_L(x)$ is the cross-sectional condensate mass flow rate in kg/s) be approximately less than 1000. Though, strictly, laminar/laminar modeling of the flow should be adequate only for $Re_{in} \leq 2100$ in order to ensure vapor laminarity, it is experimentally found that (see [9]) the assumption of "near interface" laminarity is all that is needed for heat transfer prediction by this model. This assumption is valid for much higher values of Re_{in} (see the sample criteria that is experimentally developed in [9] for the flow of FC-72).

Details, trends, and projections for the surfaces $\sum_1$ and $\sum_2$ in Fig. 6a

The transition between gravity dominated region (right of $\sum_2$) and the purely shear driven region (left of $\sum_1$) as represented in Fig. 6a is now described. This description needs the help of the subsequent Figs. 6b–6d.

The map in Fig. 6a is obtained by: (i) first selecting representative values of $Ja/Pr_1 = 0.004$, $\rho_2/\rho_1 = 0.0148$, and $\mu_2/\mu_1 = 0.0241$ which is within the cubical neighborhood of $\{Ja/Pr_1, \rho_2/\rho_1, \mu_2/\mu_1\}$ given in Eq. (28), and (ii) by considering transitions between entirely gravity and entirely shear driven flows in the three-dimensional $\{x, Re_{in}, G_p\}$ space. In this space, a solution for 0g ($G_p = 0$), under pure shear conditions, has a non-dimensional film thickness profile, denoted as $\delta_{ps}(x)$. A representative profile of $\delta_{ps}(x)$ along with a 4% neighborhood (shown by dotted lines) is shown in Fig. 6b. When the gravity parameter G_p is gradually increased to non-zero positive values (this could happen by allowing gravity vector in Fig. 1b to become non-zero or by inclining the horizontal channel in Fig. 1a), it is found that over a certain downstream distance $x > x^*$, the shear driven flow starts exhibiting a departure greater than 4% from the $G_p = 0$ case. Typically, this x^* value reduces as G_p increases. This x^*, when plotted as $x^* = x^*(Re_{in}, G_p)$, yields the surface Σ_1 in Fig. 6a. The curves bounding the surface Σ_1 in Fig. 6a arise from the constraints $0 < x^* \leq x_{0.7}$ and $0 \leq Re_{in} \leq 7000$.

A representative profile of $\delta_{Nu}(x)$ in Eq. (26) along with a 4% neighborhood (shown by dotted lines) is shown in Fig. 6c. If the parameters are such that the flow's film thickness predictions are within this neighborhood, the flow is said to be gravity dominated or entirely gravity driven. If for any given parameter set in the gravity dominated region, G_p is reduced or Re_{in} is increased, a point x^{**} appears near the inlet in Fig. 6c and is marked by the fact that the effects of shear in the region $0 \leq x \leq x^{**}$ causes a departure greater that 4% from the $\delta_{Nu}(x)$ behavior. This x^{**} increases as G_p is further reduced (or Re_{in} is further increased). This x^{**}, when plotted as $x^{**} = x^{**}(Re_{in}, G_p)$, yields the surface Σ_2 in Fig. 6a. The curves bounding the surface Σ_2 in Fig. 6a arise from the constraint $0 < x^{**} \leq x_{0.7}$ and $0 \leq Re_{in} \leq 10000$.

Therefore, in the shear driven flow zone (left of surface Σ_1 in Fig. 6a or left of its projection – termed *zone B* - in Fig. 6d), where $\delta(x) \approx \delta_{PS}(x)$, the following equation is satisfied:

$$\text{for } 0 < x < x_{0.7}, \quad \left|\frac{\delta(x)-\delta_{PS}(x)}{\delta_{PS}(x)}\right| < 0.04 . \tag{29}$$

Similarly, in the gravity dominated flow zone (right of surface Σ_2 in Fig. 6a or right of its projection – termed *zone A* – in Fig. 6d), where $\delta(x) \approx \delta_{Nu}(x)$, the following equation is satisfied:

$$\text{for } 0 < x < x_{0.7}, \quad \left|\frac{\delta(x)-\delta_{Nu}(x)}{\delta_{Nu}(x)}\right| < 0.04 \tag{30}$$

As shown in Fig. 6a, operating conditions on surface Σ_1 itself (i.e. *zone B* in Fig. 6d) are such that, over the leading part ($0 < x < x^*$), the condensate film is affected by shear whereas, over the aft portion ($x^* < x < x_{0.7}$), gravity effects start playing a role. Thus for these operating conditions, the following conditions hold:

$$\text{for } 0 < x < x^*, \quad \left|\frac{\delta(x)-\delta_{PS}(x)}{\delta_{PS}(x)}\right| < 0.04$$

$$\text{while for } x^* < x < x_{0.7}, \quad \left|\frac{\delta(x)-\delta_{PS}(x)}{\delta_{PS}(x)}\right| \geq 0.04 \tag{31}$$

Similarly for operating conditions on surface Σ_2 (i.e. *zone A* in Fig. 6d) are such that, over the leading part ($0 < x < x^{**}$), the condensate film is affected by shear whereas, over the aft portion ($x^{**} < x < x_{0.7}$), gravity effects remain dominant. Thus for these operating conditions, the following criteria hold:

$$\text{for } 0 < x < x^{**}, \quad \left|\frac{\delta(x)-\delta_{Nu}(x)}{\delta_{Nu}(x)}\right| > 0.04$$

$$\text{while for } x^{**} < x < x_{0.7}, \quad \left|\frac{\delta(x)-\delta_{Nu}(x)}{\delta_{Nu}(x)}\right| \leq 0.04 \tag{32}$$

The region between surfaces Σ_1 and Σ_2 in Fig. 6a (i.e. between *zone A* and *zone B* in Fig. 6d) define "mixed" driven flows for which both shear and gravity are important to varying degrees. This transitional zone is characterized by the set of following two equations that hold for all x ($0 < x < x_{0.7}$):

$$\left|\frac{\delta(x)-\delta_{Nu}(x)}{\delta_{Nu}(x)}\right| > 0.04 \text{ and } \left|\frac{\delta(x)-\delta_{PS}(x)}{\delta_{PS}(x)}\right| > 0.04 \tag{33}$$

Recall that $\delta_{ps}(x)$ is the film thickness obtained for the purely shear driven flows under zero gravity conditions. These $\delta_{ps}(x)$ values for the internal condensing flows in the annular/stratified regime can be correlated and are useful because, as shown in [10], these 0g or horizontal channel annular flows can be realized up to a certain downstream distance provided the hardware arrangement for the flows' realization gives the flow an ability to self-seek its "natural" exit condition in an undisturbed fashion. These flows are more robustly achieved by "actively" controlling the flow to hold the exit condition near its "natural" self-sought steady value. If this is not done, shear driven flows often exhibit more complex morphologies ([17]-[19]). We report here a computationally obtained correlation of the solutions obtained from the 1-D approach for $Fr^{-1}_x = 0$ (i.e. $G_p = 0$) while the remaining non-dimensional parameters continue to be in the range given in Eq. (28). The correlations are within 8% of the numerical solutions for the film thickness $\delta_{ps}(x)$ (or for the local heat transfer coefficient h_x through $Nu_x \equiv h_x \cdot L_c/k \approx 1/\delta(x)$) and the point of 75% condensation (i.e. $x = x_{0.75}$). They are given as:

$$\delta_{ps}(x) = \frac{0.7487 * x^{0.35} * (Ja/Pr_1)^{0.3611} * (\rho_2/\rho_1)^{0.2380}}{Re_{in}^{0.3529} * (\mu_2/\mu_1)^{0.5947}}$$

$$x_{0.75} = \frac{0.0447 * Re_{in} * (\rho_2/\rho_1)^{0.43} * (\mu_2/\mu_1)^{0.49}}{(Ja/Pr_1)^{0.9}} \tag{34}$$

Even though the impact of the temperature difference variable ΔT (i.e. its non-dimensional form Ja/Pr_1) on the surface Σ_1 and Σ_2 is important, it is not clearly depicted through Fig. 6a (because it is for a specific value of ΔT). Thus, we project Fig. 6a on $Re_{in} - G_p$ plane and obtain Fig. 6d. For each Ja/Pr_1, we take the left most line of Zone-B and right most line of Zone-A in Fig.6d (which are, respectively, projections of Σ_1 and Σ_2 of Fig. 6a) and then, using these lines, construct the surfaces Σ_S and Σ_G in the $\{Re_{in}, G_p, Ja/Pr_1\}$ space. This is done and shown in Fig. 7a.

Now Fig. 7a shows that, for any given fluid (ρ_2/ρ_1 and μ_2/μ_1values) one can think of the "narrow" region to the left of Σ_S as the region for which the flow is shear driven at all x, Re_{in}, and Ja/Pr_1 of interest. Similarly, one can think of the "large" region to the right of Σ_G in Fig. 7a as the region for which the flow is "gravity dominated" at all x, Re_{in}, and Ja/Pr_1 of interest. To

better understand the impact of the temperature difference ΔT (i.e. Ja/Pr_1) on the curvature of the surfaces Σ_S and Σ_G of Fig. 7a, the surfaces' projections on Re_{in}-G_p plane is shown in Fig. 7b.

The above described transition maps for annular flows significantly enhance similar investigative interests of Chen, Gerner, and Tien [24]. This paper makes both the criteria and the needed results accessible through the 1-D approach described here.

As the experimental/computational knowledge of the actual parametric boundaries for realizing annular/stratified flows become available through further research, the transition maps for annular/stratified flows shown in Fig. 7a can incorporate and show these boundaries. Furthermore, such maps can then be presented in a fashion that these graphical results can be generated for a range of $\{\rho_2/\rho_1, \mu_2/\mu_1\}$ values of interest to the user. After the flows' sensitivities are better understood, a more general purpose correlation for the "mixed" driven flow region can also be proposed.

6. SUMMARY OF PROPOSED CORRELATIONS AND TRANSITION MAPS FOR ANNULAR/STRATIFIED FLOWS AND THEIR RELATIONSHIP TO EXPERIMENTS

6.1 Summarized Correlations

For "near interface" laminar conditions in the vapor and the liquid, the modeling in this paper is adequate provided the wave amplitudes are not significant, the annular flows are stable and experimentally realized in a way that is cognizant of these flows' different sensitivities ([9]-[10]) to externally imposed time-varying exit condition, etc. For a quick estimate of the key trends for such quasi-steady annular flows, we recommend the following:

(i) For purely shear driven flows (left of Σ_1 in Fig. 6a or left of Σ_S in Fig. 7a), the recommendation for heat transfer coefficient h_x is:

$$Nu_x = \frac{h_x L_c}{k_1} = \frac{1}{\delta_{ps}(x)}, \tag{35}$$

where $\delta_{ps}(x)$ and $x_{0.75}$ are given by Eq.(34).

(ii) For gravity dominated flows (right of Σ_2 in Fig. 6a or right of Σ_G in Fig. 7a), the definition for heat transfer coefficient h_x in Eq. (35) remains the same, except that $\delta_{ps}(x)$ is replaced by $\delta_{Nu}(x)$ given by the Nusselt correlation in Eq. (26).

(iii) For a "mixed" driven annular flow marked by the purple shaded domain in Fig. 6d (which is mostly gravity dominated), the heat transfer coefficient h_x (in $Nu_x \equiv (h_x L_c/k_1) = 1/\delta(x)$) and $x_{0.75}$ can be obtained from:

$$\delta(x) = \frac{15.93 * x^{0.26} * (Ja_1/Pr_1)^{0.2684} * (\rho_2/\rho_1)^{0.8065}}{Re_{in}^{0.8056} * (\mu_2/\mu_1)^{0.8426} * (Fr_x^{-1})^{0.3891}}$$

$$x_{0.75} = \frac{2.69 * Re_{in}^{0.1826} * (\rho_2/\rho_1)^{1.1695} * (\mu_2/\mu_1)^{0.1085}}{(Ja_1/Pr_1)^{0.9911} * (Fr_x^{-1})^{0.5334}} \tag{36}$$

Better correlations for this "mixed" driven flow is possible but is not attempted here.

6.2 Experimental viability for purely shear driven flows

Purely shear driven flows in the geometries of Figs. 1a–b occur in 0g, in the horizontal channel configuration of Fig. 1a (with $\alpha = 0$ and $g_y = -9.81$ m/s²), and, as shown later in section 8 of this paper, in the μm-scale duct geometries of modern interest.

Quantitative comparison for the results given here is currently not possible for the experimental results given in [10] because the experimental flow geometry (Fig. 5 in [10]) is different from the one considered here. Comparisons between theory and experiments for shear driven annular/stratified flow are, however, expected in the near future.

The reader should be cautioned that typical horizontal tube experimental results available in the literature for mm or larger scale horizontal tubes (such as [16]) are not in any of the above categories of purely shear driven annular flows, or gravity dominated annular flows, or "mixed" driven annular flows. This is because these flows are often three-dimensional in nature (except when vapor flows are fast and the flow is annular) where both forward shear and azimuthal gravity component are important.

The reader should also be careful in concluding that horizontal channel experimental data for hydraulic diameters that are mm scale or larger are always "shear driven" cases. This may not be the case because of the following:

(i) If the experimental arrangement shows even ± ½° or more inclination, interfacial shear forces on the condensate become quite weak (if $D_h \geq 4$ mm for the flows considered here) relative to the more dominant gravitational forces.

(ii) The pure-shear zone is small in Fig. 7a, and one typically has to operate at very small G_p and sufficient large Re_{in} to ensure that one is operating within or near the purely shear driven annular flow regime.

Because of the above described sensitivity/limitations with large hydraulic diameter horizontal channel condensing flows, it was found that the large hydraulic diameter rectangular cross-section (w = 40 mm, h = 25 mm) test-section of 0.9 m length used in the experiments of Lu and Suryanarayana [14] do not relate to the intended investigations of purely shear driven cases. In fact the results are in near perfect agreement (see section 6.3) with entirely gravity driven or gravity dominated cases. This observation follows from the hypothesis that the experimental uncertainties caused their channel's bottom condensing-surface (see Fig. 1a) to be tilted downward by an angle of $\alpha = 1°$. The comparisons between the proposed theory and experiments under this hypothesis for their runs ([14]-[15]) are presented in the next section. A private correspondence with the senior author of [14] also states that they only ensured the horizontalness of the top surface of their test-section and that the condensing-surface itself might have had a 1° downward tilt.

6.3 Comparisons with experiments for "gravity driven/dominated" annular flow situations

The modeling results presented in this paper for gravity dominated (Nusselt result in Eq. (26)) as well as gravity driven (such as in Eq. (36)) cases agree very well with our experimental data, reported in [9], for condensation of FC-72 in a vertical tube. We refer the reader to [9] for a more comprehensive discussion of the range of experimental conditions for which this smooth interface laminar/laminar theory is found to be adequate.

Besides the vertical tube experimental results discussed in [9], as remarked in section 6.2, relevant experimental results obtained from the slightly tilted ("so called" horizontal) channel also meet the requirement of being annular/wavy, laminar/laminar, and gravity driven. This is because the condensing-surface in Lu and Suryanarayana [14], when assumed to have an unintended downward inclination of $\alpha = 1°$ (see Fig. 1a), has most of its data in excellent agreement with the theory presented here. Under this assumption, the comparison of their film thickness and average heat transfer coefficient data is shown in Table 1 for representative flows of FC-72 and in Table 2 for representative flows of R113. Lu and Suryanarayana [14] data are also close to the Nusselt regime – right of Σ_G in Fig. 7a – hence the agreement of their data with the Nusselt result (Eq. (26)) is also quite good (though not as good as the full theory). Lu and Suryanarayana [14] experimental runs involved only partial condensation and hence heat transfer rates were calculated from Eq. (1) in [9] with Table-1's parameter space being

$$9285.3 \leq Re_{in} \leq 35284.7,\ 0.0243 \leq Ja/Pr_1 \leq 0.0909,\ 0.0080 \leq \rho_2/\rho_1 \leq 0.0086$$

$$0.0459 \leq \mu_2/\mu_1 \leq 0.0472,\ 3198304 \leq G_p \leq 3651997 \tag{37}$$

and Table-2's parameter space being

$$5358.71 \leq Re_{in} \leq 28918.56,\ 0.0130 \leq Ja/Pr_1 \leq 0.0275,\ 0.0047 \leq \rho_2/\rho_1 \leq 0.0057$$

$$0.0171 \leq \mu_2/\mu_1 \leq 0.0226,\ 1122008 \leq G_p \leq 1518915 \tag{38}$$

A graphical comparison of average heat transfer coefficient obtained by their experiment ([14]) and the proposed theory is presented in Fig. 8. With increased waviness, for reasons described in [9], the experimental heat transfer coefficients may be larger than 15% of the theoretical value. Unlike our full condensation data in [9], for these partial condensation channel flow situations, there is not enough data in [14] to construct boundaries for the data that exceeds the proposed model's heat-transfer coefficient predictions by more than 15% or 30%.

7. THE 1-D APPROACH'S ABILITY TO HANDLE DIFFERENT CONDENSING-SURFACE THERMAL BOUNDARY CONDITIONS FOR DIFFERENT METHODS OF COOLING

For many conjugate heat transfer problems, the thermal boundary condition for the condensing surface temperature $T_w(x)$ or heat-flux $q_w''(x)$ needs to be initially assumed and subsequently these assumed values needs to be iteratively corrected (until convergence) by checking their compatibility with the solution (or realization) of the adjoining conjugate heat transfer problem (s). As an example, after assuming a thermal temperature boundary condition $T_W(x)$ for the condensing-surface, the condensing surface problem is solved and heat-flux variation $q_w''(x)$ is found. This $q_w''(x)$ then becomes the boundary condition for the conjugate heat-transfer problem which is then solved and the solution of this conjugate problem yields a new value of $T_w(x)$ for the condenser-surface. With this new condensing-surface temperature boundary condition $T_w(x)$, the condensing flow problem needs to be solved again. The process of solving the condensation flow problem and the conjugate problem needs to be iterated until mutually consistent and convergent thermal boundary conditions for the condensing-surface is obtained. For the above reason, it is important to demonstrate the ability to solve a condensing flow problem for any known uniform or non-uniform thermal boundary condition of $T_w(x)$ or $q_w''(x)$.

In Fig. 9a, curve-A depicts an assumed $\Delta T(x) \equiv T_{sat}(p_{in}) - T_w(x)$ for a certain non-uniform condensate surface temperature $T_w(x)$. Our simulation methodology described in section-2 for variable wall temperature yields the film-thickness $\delta(x)$ curve in Fig. 9b as well as the values of $q_w''(x)$ (in W/m²) shown as curve-B in Fig. 9a. The fact that this prediction methodology for a known $\Delta T(x)$ as well as the prediction methodology described in section-2 for variable wall heat-flux $q_w''(x)$ are both good is demonstrated next. We use the output of $q_w''(x)$ from the variable wall temperature case (curve-B in Fig. 9a) as the input "known" wall heat-flux for the variable heat-flux methodology of section-2. This yields two results: (i) the film thickness $\delta(x)$ curve shown in Fig. 9b, and (ii) $\Delta T(x) \equiv T_{sat}(p_{in}) - T_w(x)$ values shown as curve-A in Fig. 9a. The fact that both the $\delta(x)$ curves in Fig. 9b and the $\Delta T(x)$ curves in Fig. 9a are identical, establishes the efficacy of our 1-D simulation approach for the important class of problems involving non-uniform thermal boundary conditions for condensing-surface. To our knowledge,

this type of simulation capability for a lower dimension 1-D technique has not been reported before and, therefore, is one of the unique contributions of this paper.

8. COMPUTATIONAL RESULTS FOR CONDENSING FLOWS IN MICROMETER SCALE DUCTS

As stated earlier, purely shear driven flows may occur in μm-scale (or large) hydraulic diameter D_h ducts regardless of the duct's orientation with respect to the gravity vector. This is because, as hydraulic diameter D_h decreases, shear and pressure forces per unit volume starts increasing and, at some low enough value of D_h, they dominate the gravitational forces per unit volume.

Consider, in Fig. 10a, a Re_{in}-G_p projection of a three dimensional result of the type shown in Fig. 6a. If one reduces the tube diameter D by letting $D \rightarrow 0$ – while average vapor inlet speed U, gravity level g_x, and ΔT are held constant – an arbitrary point A_2 moves along the curve C in Fig. 10a to point B_2. At sufficiently small diameter $D = D_{cr}$, the pure shear boundary zone B (of Fig. 6d) is fully crossed for the Ja/Pr_1 value under consideration. This is illustrated by the fact that, for point A_2 in Fig. 10a (which marks a 1g situation for a vertical tube of diameter D), the corresponding 0g situation is point A_1. Since $D > D_{cr}$ associated with the transition to shear driven flows, the 1g (A_2) and 0g (A_1) flows are quite different. This difference is clearly seen through film thickness simulation results (shown in Fig. 10b) for point A_1 and A_2. However, for cases marked by points B_1 and B_2 in Fig. 10a, the 1g point B_2 has a corresponding 0g point B_1. Since both these flows are for diameters of the tube $D \leq D_{cr}$, the simulation results for these flows are nearly identical (again see Fig. 10b) as both the flows have a gravitational parameter which is at or near zero and condensate flow is shear driven in nature. As a result, one finds that for $D < D_{cr}$ (which is nearly equal to 0.3 mm and could be in μm range if a different curve C was chosen for a different U and ΔT), the flow becomes shear driven (see Fig. 10b). Despite this, for this gravity insensitive behavior there may often be a serious penalty of large pressure drops (see Fig. 10c) and high pumping powers across the length of such mm- or μm-scale condensers. However if a designer of a two-phase thermal system for an aircraft chooses the tube diameter

D_{cr} and its operating conditions properly (e. g. in the region left of zone B in Fig. 10a), the condenser performance could be both acceptable as well as gravity-insensitive.

As a result of significant changes in pressure drop values (Fig. 10c) along with the changes in the other flow features, it should be noted that some new issues – that are ignored in the proposed theory - have become important for these "$D < D_{cr}$" μm-scale flows. These new issues are: (i) variations in interfacial saturation temperature $T_{sat}(p_2^i)$ may become non-negligible as variations in interfacial pressure p_2^i have become significant, (ii) vapor's density variation (compressibility) became important because of the large pressure drop, (iii) liquid-vapor surface tension effects may become important because of the large curvature at the interface (as one of the radii of the curvature is of the same order of magnitude as D_{cr} /2), and (iv) liquid-solid surface energy issues ("disjoining pressure," etc.) may become important over a certain range of film thickness values depicted in Fig. 10b. The last liquid-solid surface energy issue may not be important for most micro-scale flows of interest. For example, if $D \leq 0.2$ mm, the film thickness variations in Fig. 10b where disjoining pressure may be important corresponds to approximate locations $0 \leq x \leq 0.02$ m where 10 nm $\leq \delta \leq$ 20 nm. Rest of the above identified issues are important and are currently being addressed and explored for μm-scale flows.

9. CONCLUSIONS

1. An effective 1-D theoretical/computational approach has been presented for solving a class of annular in-tube and in-channel condensing flows for different thermal boundary conditions.
2. Computational results presented in this paper highlight the significant differences between steady gravity driven and steady shear driven annular flows as far as flow features are concerned.
3. The results regarding the proposed transition maps (which are helpful in ascertaining whether the annular flow is entirely gravity driven, purely shear driven or mixed) are very useful for ascertaining transition between gravity and shear driven annular stratified flows. In this paper these transition maps are presented for a large range of parameters and this should be useful for estimates in the design of certain experiments and applications. The maps also highlight the need for presenting the boundary of annular

flows within the context of the non-dimensional parameters (with or without some variations) considered here.

4. For mm-scale range, the results from 1-D solution technique were validated by successful comparisons with 2-D results. The 1-D computational results also showed good agreement with the corresponding experimental results for gravity driven cases (see [9]). Thus, annular flow zones shown in Fig. 6a and correlations in Eqs. (34) and (36) should be considered reliable and representative of other correlations that can be developed by the method given here.
5. It is also shown that, under certain conditions, the results presented for cylindrical geometry could be related to results for channel geometry.
6. The shear driven or 0g correlation in Eq. (34) for annular/stratified flows (zone to the left of surface Σ_S in Fig. 6a) is an important quantitative result for design and operation of condensers in space. However, such shear driven flows are much more geometry dependent that the gravity driven flows. The quantitative uniqueness and attainability of shear driven flows, along with various sensitivities of these flows (see [9], [10]) have been demonstrated by our experiments [10]. These results are important for effective use of condensers in space-based or μm-scale applications.

ACKNOWLEDGEMENT

This work was supported in parts by NASA grant NNC04GB52G and NNX10AJ59G and NSF grant NSF-CBET-1033591. The authors would like to thank Sushant More for his assistance in preparation of this manuscript.

REFERENCES

[1] Carey, V. P., 1992, *Liquid-Vapor Phase-Change Phenomena*, Series in Chemical and Mechanical Engineering, Hemisphere Publishing Corporation.

[2] A. Narain, S. D. Kulkarni, S. Mitra, J. H. Kurita, M. Kivisalu, Computational and Ground Based Experimental Investigations of the Effects of Specified and Unspecified (Free) Pressure Conditions at Condenser Exit for Condensing Flows in Terrestrial and Micro-Gravity Environments, Annals of New York Academy of Sciences, Interdisciplinary Transport Phenomenon, 2008.

[3] A. Narain, J. H. Kurita, M. Kivisalu, S. D. Kulkarni, A. Siemionko, T. W. Ng, N. Kim, L. Phan, Internal Condensing Flows Inside a Vertical Pipe – Experimental/Computational Investigations of the Effects of Specified and Unspecified (Free) Conditions at Exit, ASME Journal of Heat Transfer (2007) pp. 1352-1372.

[4] Q. Liang, X. Wang, A. Narain, Effect of Gravity, Shear and Surface Tension in Internal Condensing Flows - Results from Direct Computational Simulations, ASME Journal of Heat Transfer 126 (5) (2004), pp. 676-686.

[5] A. Narain, Q. Liang, G. Yu, X. Wang, Direct Computational Simulations for Internal Condensing Flows and Results on Attainability/Stability of Steady Solutions, Their Intrinsic Waviness, and Their Noise-Sensitivity, Journal of Applied Mechanics 71 (2004) pp. 69-88.

[6] L. Phan, X. Wang, A. Narain, Exit Condition, Gravity, and Surface-Tension Effects on Stability and Noise-sensitivity Issues for Steady Condensing Flows inside Tubes and Channels, International Journal of Heat and Mass Transfer 49 Issues 13-14 (2006) pp. 2058-2076.

[7] L. Phan, A. Narain, Non-linear Stability of the Classical Nusselt Problem of Film Condensation and Wave-Effects, ASME Journal of Applied Mechanics 74 (2) (2007), pp. 279-290.

[8] S. D. Kulkarni, A. Narain, S. Mitra, Forced Flow of Vapor Condensing over a Horizontal Plate (Problem of Cess and Koh*) – Steady and Unsteady Solutions of the Full 2D Problem, ASME *Journal of Heat Transfer*, Vol. 132 (10), 101502, 2010.

[9] J. H. Kurita, M. Kivisalu, S. Mitra, R. Naik, A. Narain, Experimental Results on Gravity Driven Condensing Flows in Vertical Tubes, their Agreement with Theory, and their Differences with Shear Driven Flows' Boundary Condition Sensitivities, Submitted for publication in *International Journal of Heat and Mass Transfer*, 2011.

[10] S. D. Kulkarni, A. Narain, S. Mitra, J. H. Kurita, M. Kivisalu, M. M. Hasan, Flow Control and Heat Transfer Enhancement Issues Resulting from Elliptic Sensitivity for Shear Driven Annular/Stratified Internal Condensing Flows, Accepted and in-press for publication in the *International Journal of Transport Processes*, 2011.

[11] F. Dobran, R. S. Thorsen, Forced flow laminar filmwise condensation of a pure saturated vapor in a vertical tube, International Journal of Heat and Mass Transfer (23) (1980), pp. 161-177.

[12] A. Narain, G. Yu, Q. Liu, Interfacial Shear Models and Their Required Asymptotic Form for Annular/Stratified Film Condensation Flows in Inclined Channels and Vertical Pipes, International Journal of Heat and Mass Transfer 40 (15) (1997), pp. 3559-3575.

[13] M. Soliman, J.R. Schuster, P.J. Berenson, A General Heat Transfer Correlation for Annular Flow Condensation, ASME J. of Heat Transfer (1968) pp. 267-276.

[14] Q. Lu, N. V. Suryanarayana, Condensation of a vapor flowing inside a horizontal rectangular duct, Journal of Heat Transfer 117 (1995), pp. 418-424.

[15] Q. Lu, An Experimental Study of Condensation Heat Transfer with Film Condensation in a Horizontal Rectangular Duct, Ph. D Thesis, Michigan Technological University.

[16] A. Cavallini, G. Gensi, D. Del Col, L. Doretti, G. A. Longo, L. Rossetto, C. Zilio, Condensation Inside and Outside Smooth and Enhanced Tubes – A Review of Recent Research, International Journal of Refrigeration 26 (2003) pp. 373-392.

[17] H.Y. Wu, P. Cheng, Condensation Flow Patterns in Microchannels, International Journal of Heat and Mass Transfer, 48, (2005), pp. 286-297.

[18] X.J. Quan, P. Cheng, H.Y. Wu, Transition from Annular to Plug/Slug Flow in Condensation in a Microchannel, International Journal of Heat and Mass Transfer, 51, (2008), pp. 707-716.

[19] J.W. Coleman, S. Garimella, Two-phase Flow Regimes in Round, Square, and Rectangular Tubes during Condensation of Refrigerant R134a, Int. J. Refrig., 26, (2003), pp. 117-128.

[20] Greenberg, M. D., 1978, *Foundations of Applied Mathematics*, Prentice Hall, New Jersey.

[21] Arnold, V. I., 1981, *Ordinary Differential Equations*, The MIT Press, Cambridge, Massachusetts.

[22] Patankar, S. V., 1980, "*Numerical Heat Transfer and Fluid Flow*," Hemisphere, Washinton DC.

[23] Incropera, F. P. and D. P. Dewitt, 2006, *Fundamentals of Heat and Mass Transfer*, Sixth Edition, Wiley.

[24] S.L. Chen, F.M. Gerner and C.L. Tien, "General Film Condensation Correlations," Experimental Heat Transfer, 1, (1987), 93-107.

FIGURE CAPTION

Fig. 1a: A schematic describing a representative condensing flow problem in a channel.

Fig. 1b: A schematic describing a representative condensing flow problem in a vertical tube.

Fig. 2a: The figure compares steady/quasi-steady solutions for a vertical channel. The solutions are obtained by 2-D and 1-D techniques for the flow of R-113 vapor with inlet speed of U = 0.41 m/s, ΔT = 5 °C, h = 0.004 m, and g_x = 9.8 m/s^2.

Fig. 2b: The figure compares steady/quasi-steady solutions obtained by 2-D and 1-D techniques for a channel under 0g conditions. The solutions are obtained for a flow of R-113 vapor with inlet speed of U = 0.6 m/s, ΔT = 5 °C, and h = 0.004 m.

Fig. 2c: The figure compares steady/quasi-steady solutions obtained by 2-D and 1-D techniques for a flow through a vertical cylinder. The solutions are obtained for a flow of

FC-72 vapor with inlet speed of U = 1.5 m/s, diameter D = 6.6 mm, ΔT = 9 °C and g_x = 9.81 m/s^2.

Fig. 3: For the flow of R113 vapor, average inlet vapor speed U = 2 m/s, ΔT = 5 °C, and g_x = 9.81 m/s^2; the figure shows the non-dimensional film thickness for a channel with gap height h = 0.004 m and for a cylinder with diameter D = 0.004 m.

Fig. 4a: Figure shows film thickness versus x variation and the y-variations of the x-component of the velocity profile (at x = 20) for gravity driven 1g and shear driven 0g flows inside a tube. The figure also shows the linearity of temperature profiles (at x = 20) for both the cases. The solutions are obtained for flow of FC-72 vapor with inlet speed of U = 0.7 m/s, ΔT = 7.5ºC, and diameter D = 6.6 mm.

Fig. 4b: For the cases shown in Fig. 4a, this figure shows the non-dimensional interfacial pressure variations with downstream distance.

Fig. 5: Figure shows the variation in film thickness ratio ($\delta(x^{\#})/\delta_{ps}(x^{\#})$) and ($\delta_{Nu}(x^{\#})/\delta_{ps}(x^{\#})$) at $x^{\#}$ = 80 with variations in G_p. The solutions are obtained for flow of FC-72 vapor with inlet speed of U = 0.7 m/s, ΔT = 7.5ºC, and diameter D = 6.6 mm.

Fig. 6a: The figure yields a division of {x, Re_{in}, G_p} space that marks a gravity dominated zone, a shear dominated zone, and a transition zones between them. The flow of FC-72 vapor inside the tube has Ja/Pr_1 = 0.004, (ρ_2/ρ_1) = 0.0148 and (μ_2/μ_1) = 0.0241.

Fig. 6b: The figure shows the 4 % rule and a distance x* by which the flows are categorized with respect to the pure shear (0g) film thickness profile $\delta_{ps}(x)$.

Fig. 6c: The figure shows the 4 % rule and a distance x by which the flows are categorized with respect to gravity dominated film thickness profile $\delta_{Nu}(x)$.**

Fig. 6d: The figure is a projection of Fig. 6a in {Re_{in} - G_p} plane and it also marks a gravity dominated zone, a shear dominated zone, and a transition zones between them.

Fig. 7a: The figure suggests the boundaries in {Ja/Pr_1, Re_{in}, G_p} space that marks a gravity dominated zone, a shear dominated zone, and a transition zones between them. The flow of FC-72 vapor has (ρ_2/ρ_1) = 0.0148 and (μ_2/μ_1) = 0.0241.

Fig. 7b: The figure is a projection of Fig. 7a in {Re_{in} - G_p} plane.

Fig. 8: The figure graphically presents the nature of agreement between theoretically and experimentally ([14]) obtained values of average heat-transfer coefficient.

Fig. 9a: For a flow of FC-72 vapor inside a vertical tube condenser with average inlet speed U = 7 m/s, diameter D = 0.002m, the figure shows the profiles of (i) vapor to condensing-surface temperature variations (curve A), and (ii) condensing-surface heat-flux variations (curve B).

Fig. 9b: For the cases shown in Fig. 9a, the non-dimensional film thickness profile predictions resulting from the solutions of the problems for variable wall temperature difference (curve A) and variable heat flux profile (curve B) as prescriptions for condensing-surface thermal boundary condition.

Fig. 10a: For the same inlet speed U and gravity (g_x), as tube diameter D→0, the parameter Re_{in} and G_p vary along the representative curve C. The curve C intersects zone B of Fig. 6d when a certain diameter D_{cr} is reached.

Fig. 10b: For the flow of FC-72 vapor with U = 3 m/s and ΔT = 3 ºC, the figure shows solutions for 1g and 0g cases for diameter D_1 = 2 mm and D_2 = 0.2 mm. For $D_1 > D_{cr}$ (≈ 0.3 mm), the figure shows two distinct solutions for 1g and 0g cases. For $D_2 < D_{cr}$ (≈ 0.3 mm), the solutions for both 1g and 0g cases are seen to have become nearly identical.

Fig. 10c: As the tube diameter becomes sub mm- to μm-scale, , the figure shows (for the FC-72 flow in Fig. 10b) a significant rise in pressure drop ($\Delta P = P_{in} - P_{exit}$) across the condenser. The pressure drop also increases with increase in inlet mass flow rates $\dot{M}_{in}$.

FIGURES

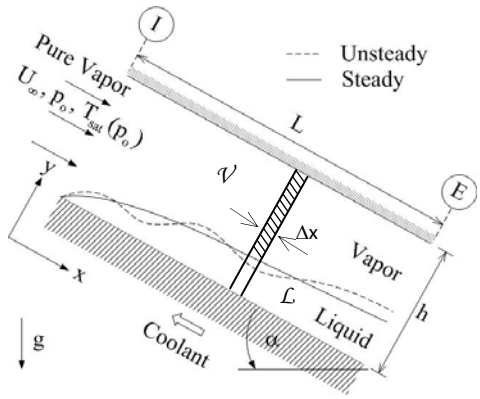

Fig. 1a

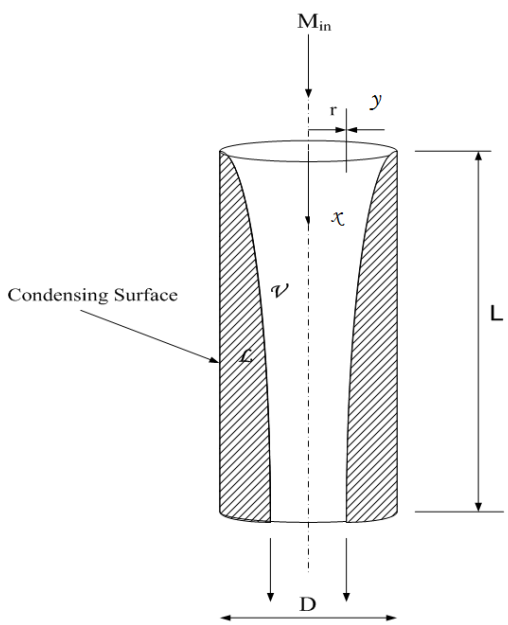

Fig. 1b

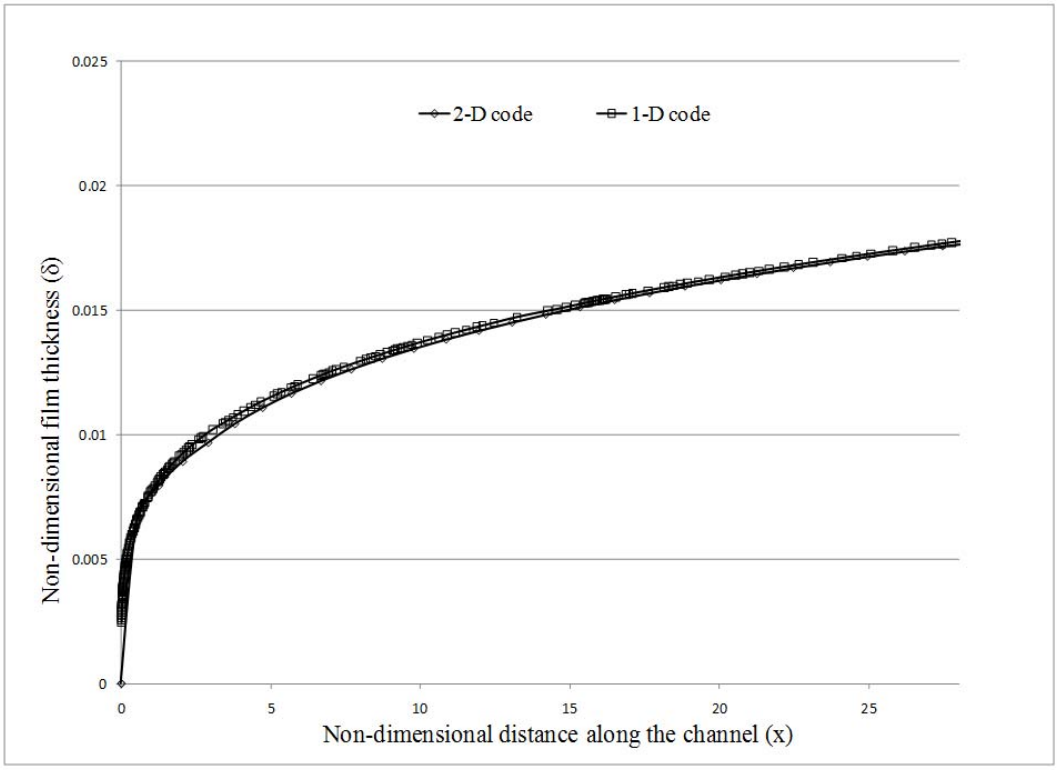
2-D code
1-D code
Non-dimensional film thickness (δ)
Non-dimensional distance along the channel (x)
0.025
0.02
0.015
0.01
0.005
0
0
5
10
15
20
25

Fig. 2a

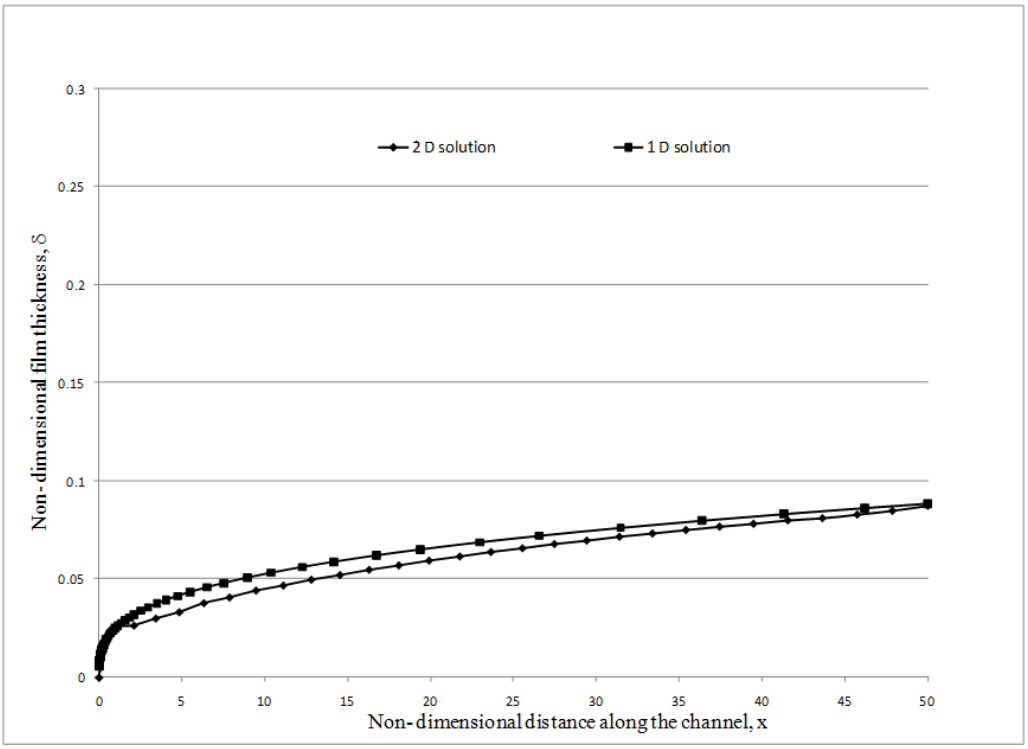
2 D solution
1 D solution
Non- dimensional film thickness, δ
Non- dimensional distance along the channel, x
0.3
0.25
0.2
0.15
0.1
0.05
0
0
5
10
15
20
25
30
35
40
45
50

Fig. 2b

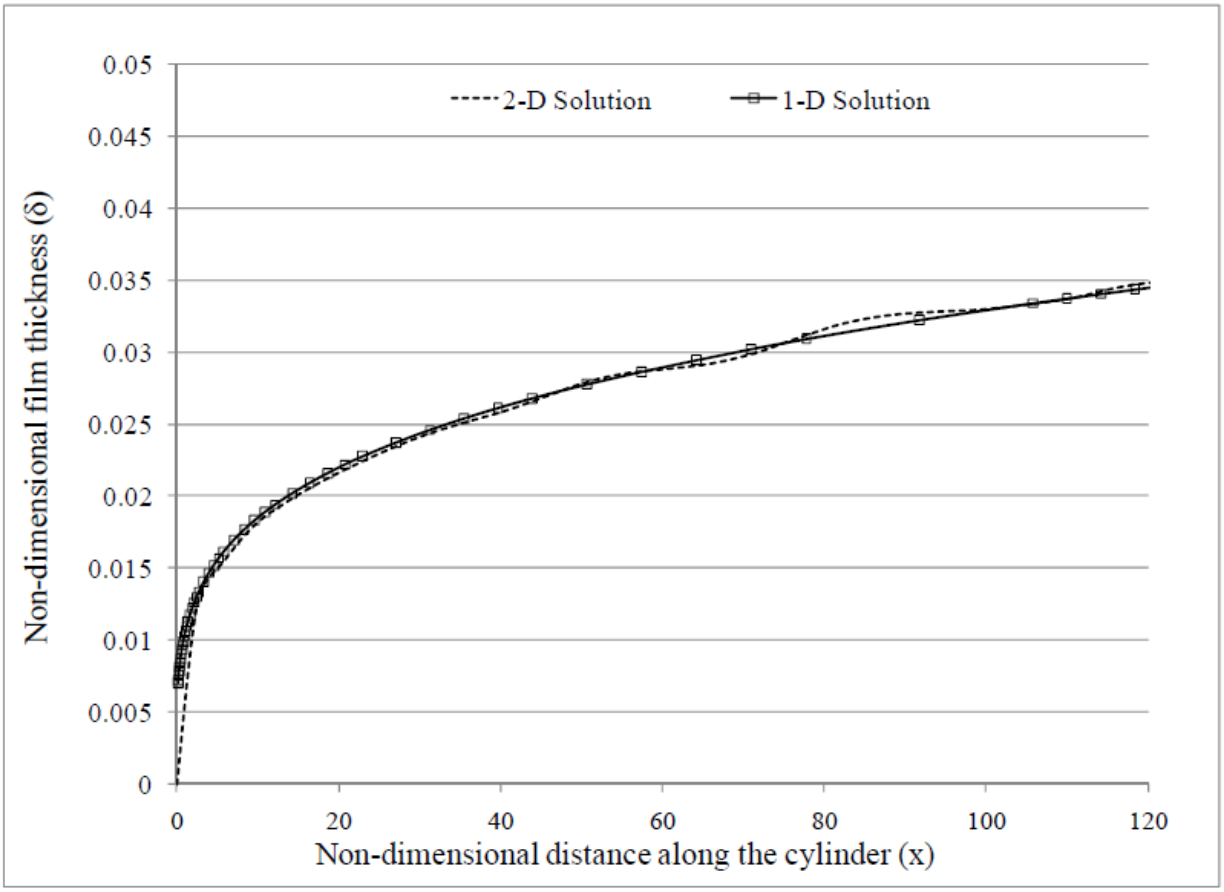
0.05
0.045
0.04
0.035
0.03
0.025
0.02
0.015
0.01
0.005
0
2-D Solution
1-D Solution
Non-dimensional film thickness (δ)
0
20
40
60
80
100
120
Non-dimensional distance along the cylinder (x)

Fig. 2c

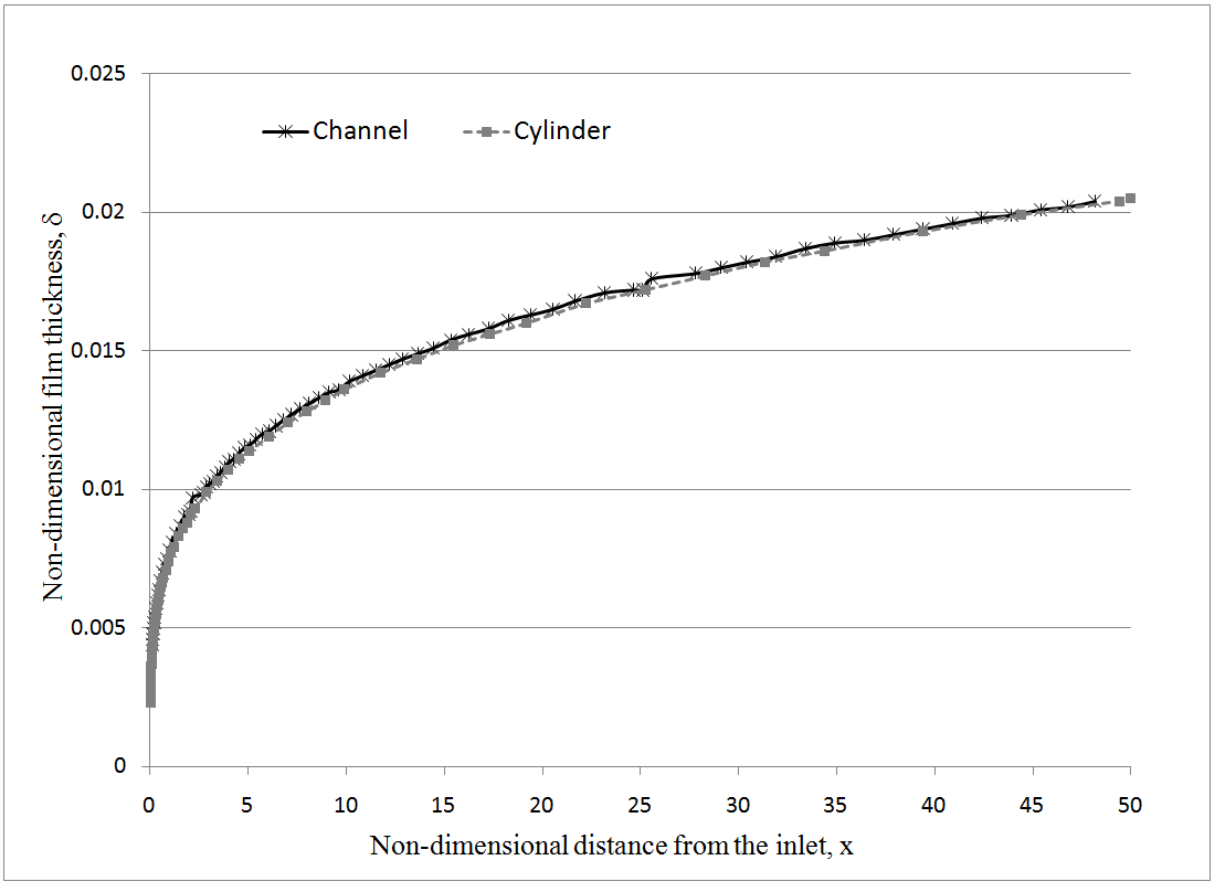
0.025
0.02
0.015
0.01
0.005
0
Channel
Cylinder
Non-dimensional film thickness, δ
0
5
10
15
20
25
30
35
40
45
50
Non-dimensional distance from the inlet, x

Fig. 3

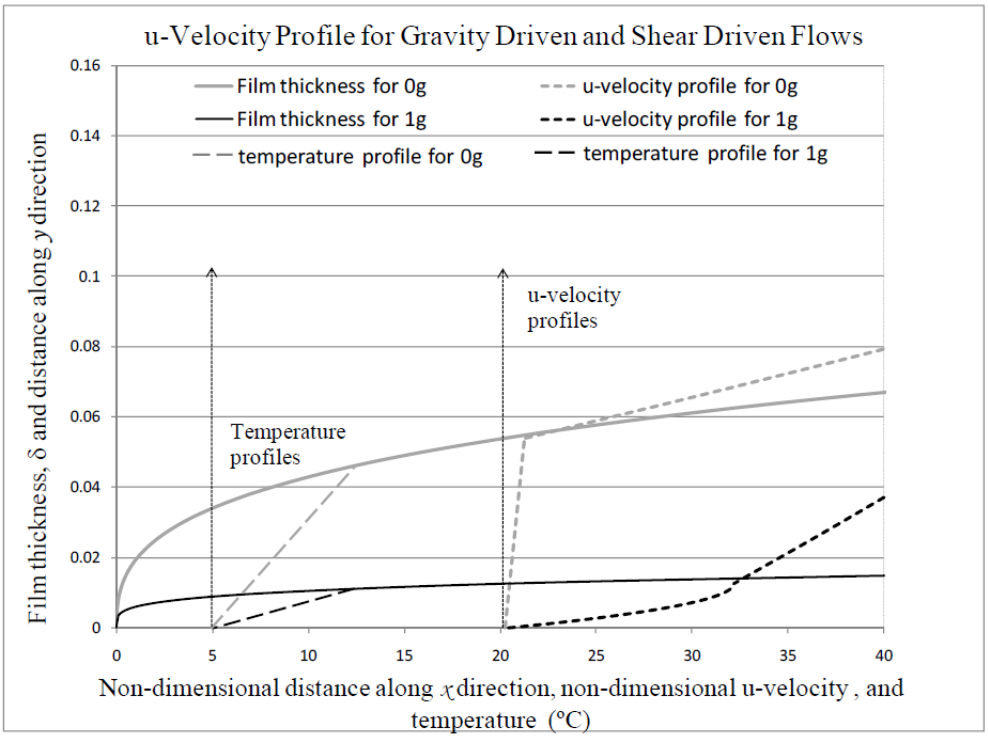
u-Velocity Profile for Gravity Driven and Shear Driven Flows
Film thickness for 0g
Film thickness for 1g
temperature profile for 0g
u-velocity profile for 0g
u-velocity profile for 1g
temperature profile for 1g
u-velocity profiles
Temperature profiles
Film thickness, δ and distance along y direction
Non-dimensional distance along x direction, non-dimensional u-velocity , and temperature (°C)
0.16
0.14
0.12
0.1
0.08
0.06
0.04
0.02
0
0
5
10
15
20
25
30
35
40

Fig. 4a

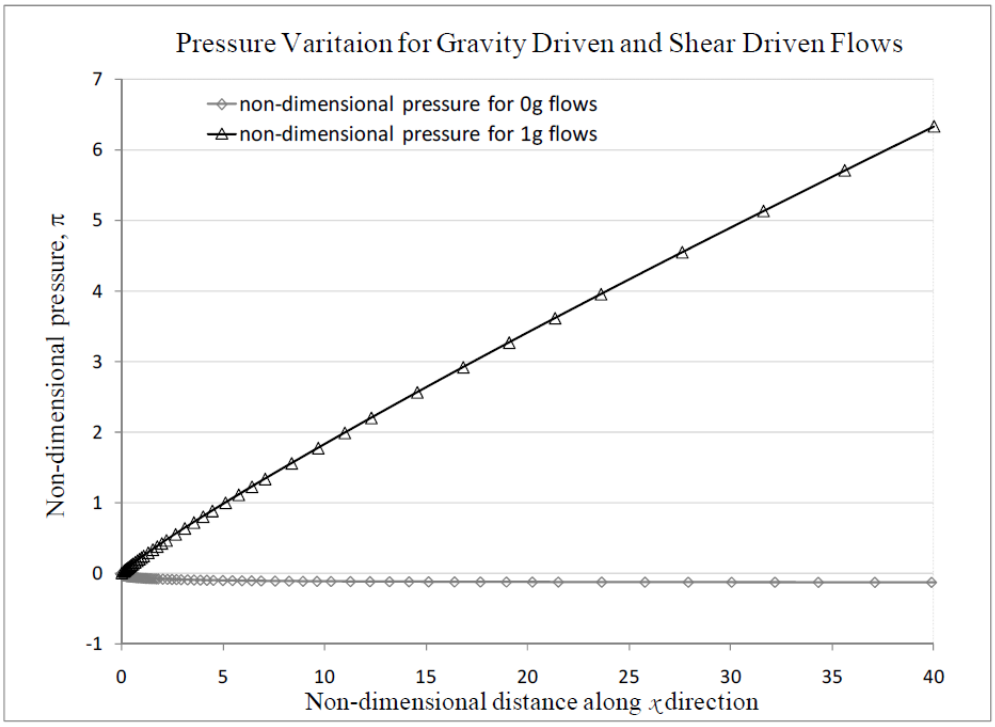
Pressure Varitaion for Gravity Driven and Shear Driven Flows
non-dimensional pressure for 0g flows
non-dimensional pressure for 1g flows
Non-dimensional pressure, π
Non-dimensional distance along x direction
7
6
5
4
3
2
1
0
-1
0
5
10
15
20
25
30
35
40

Fig. 4b

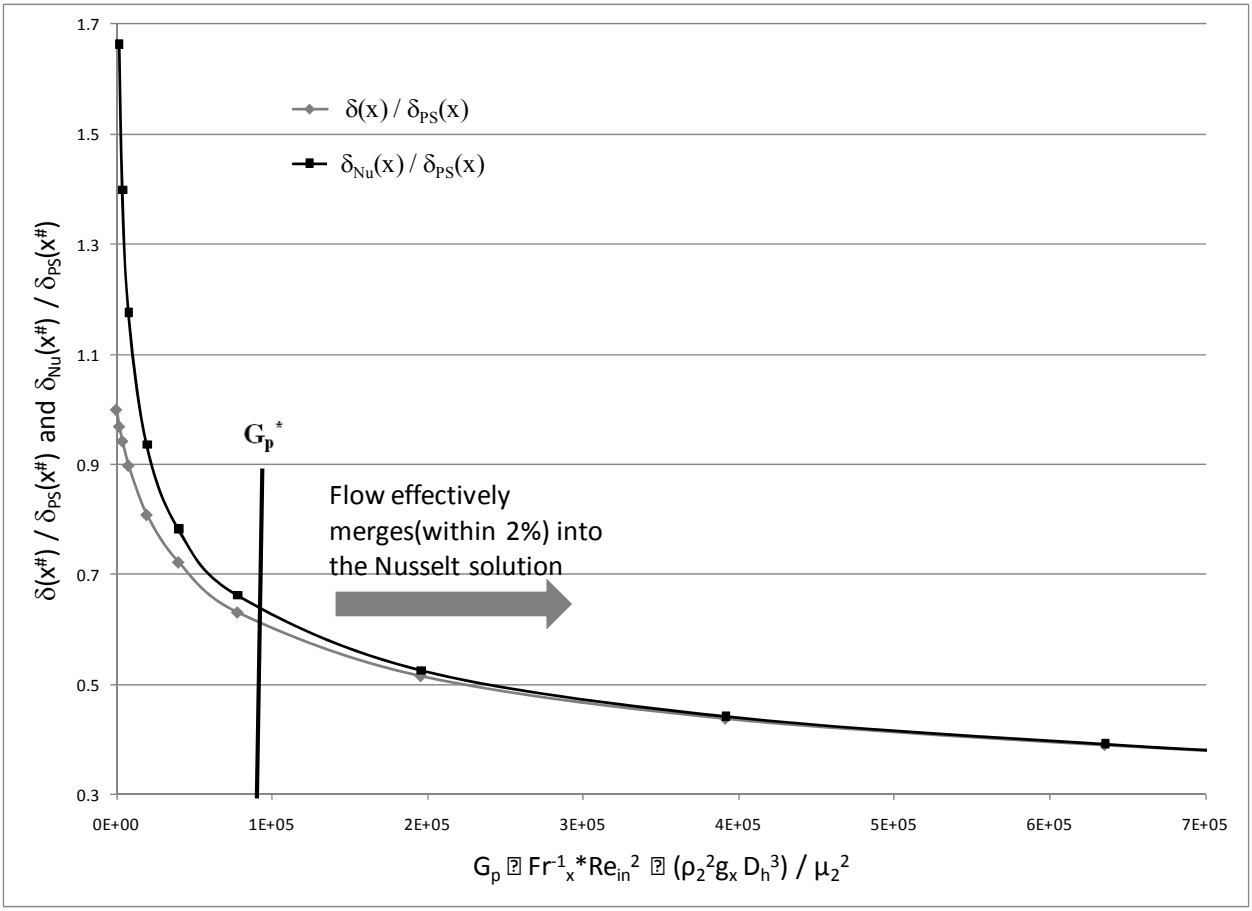
1.7
1.5
1.3
1.1
0.9
0.7
0.5
0.3
δ(x) / δPS(x)
δNu(x) / δPS(x)
Gp*
Flow effectively
merges(within 2%) into
the Nusselt solution
δ(x#) / δPS(x#) and δNu(x#) / δPS(x#)
0E+00
1E+05
2E+05
3E+05
4E+05
5E+05
6E+05
7E+05
Gp ⊠ Fr-1x*Rein2 ⊠ (ρ22gx Dh3) / μ22

Fig. 5

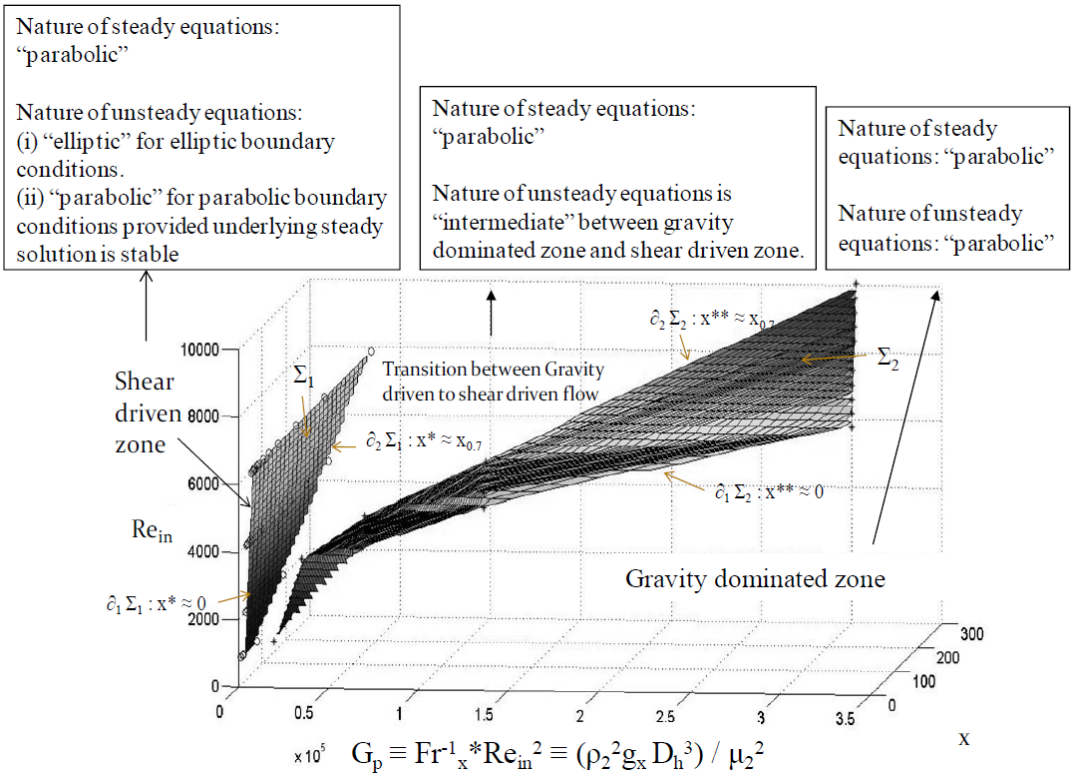
Nature of steady equations: "parabolic"
Nature of unsteady equations:
(i) "elliptic" for elliptic boundary conditions.
(ii) "parabolic" for parabolic boundary conditions provided underlying steady solution is stable
Nature of steady equations: "parabolic"
Nature of unsteady equations is "intermediate" between gravity dominated zone and shear driven zone.
Nature of steady equations: "parabolic"
Nature of unsteady equations: "parabolic"
Shear driven zone
Re_in
Σ1
Σ2
Transition between Gravity driven to shear driven flow
∂2 Σ2 : x** ≈ x0.7
∂2 Σ1 : x* ≈ x0.7
∂1 Σ2 : x** ≈ 0
∂1 Σ1 : x* ≈ 0
Gravity dominated zone
x
x 10^5 Gp ≡ Fr^-1_x*Re_in^2 ≡ (ρ2^2 gx Dh^3) / μ2^2

Fig. 6a

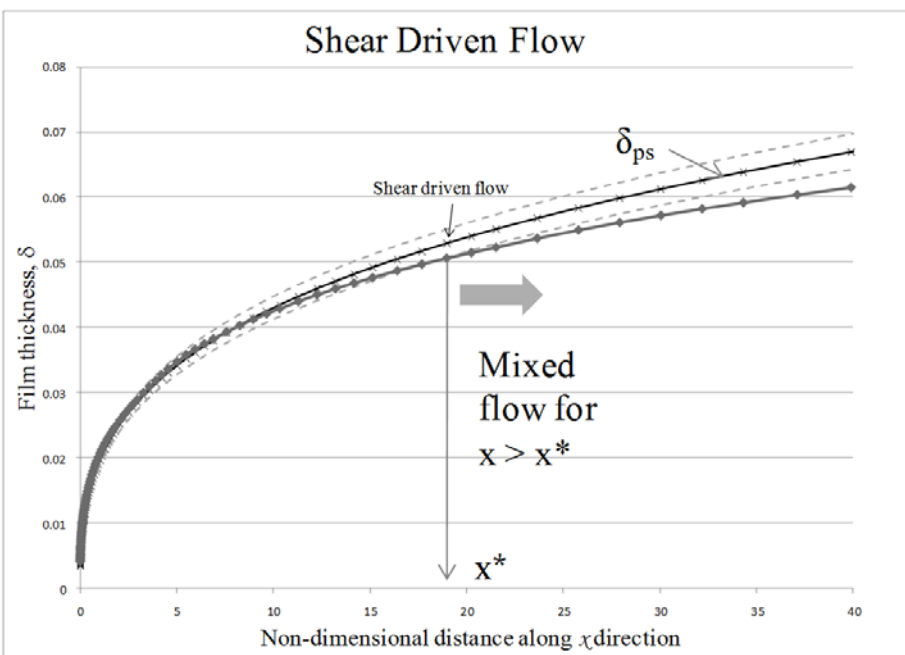
Shear Driven Flow
Film thickness, δ
Non-dimensional distance along x direction
δps
Shear driven flow
Mixed flow for x > x*
x*

Fig. 6b

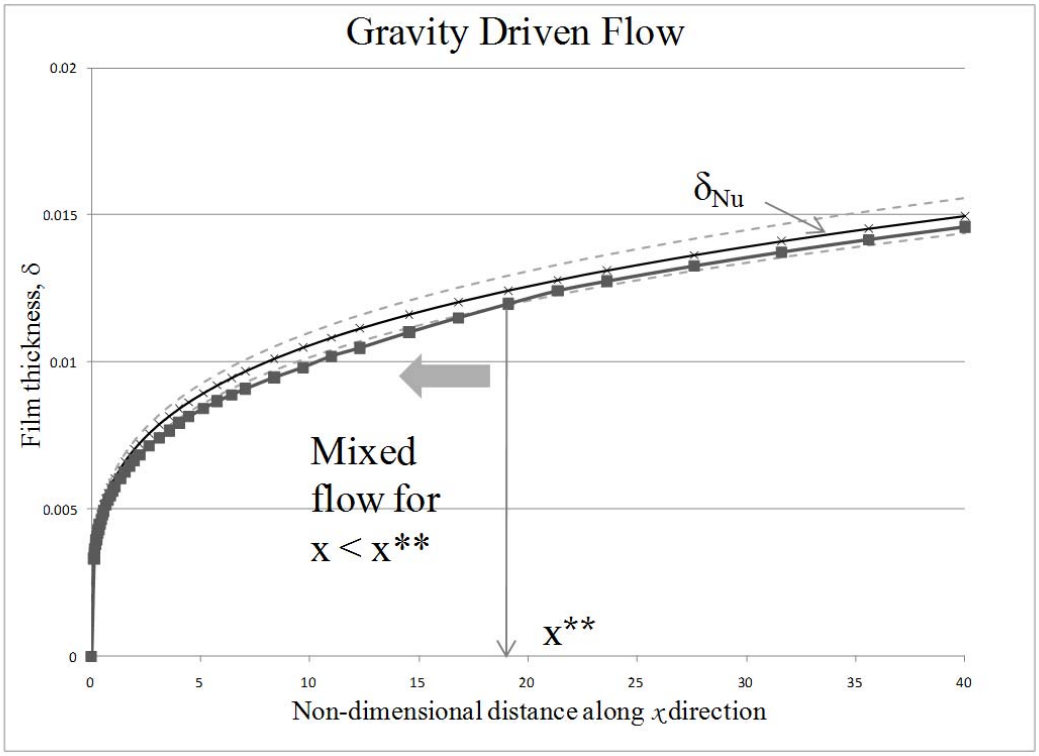
Gravity Driven Flow
Film thickness, δ
Non-dimensional distance along x direction
δNu
Mixed flow for x < x**
x**
0.02
0.015
0.01
0.005
0
0
5
10
15
20
25
30
35
40

Fig. 6c

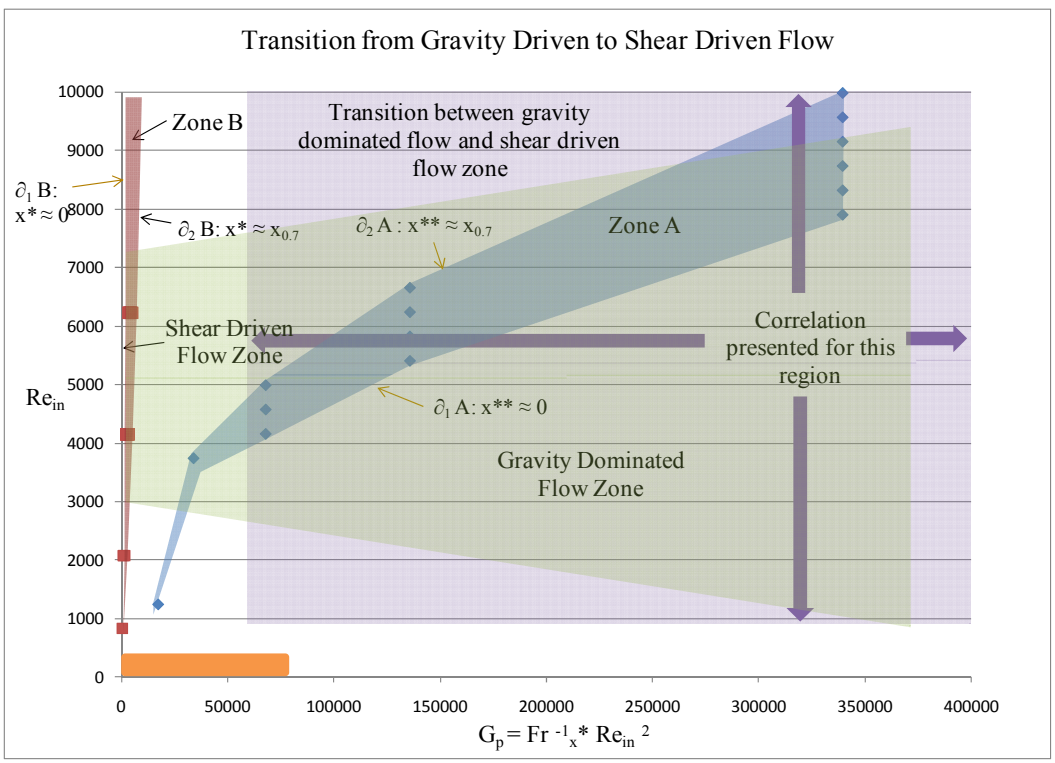
Transition from Gravity Driven to Shear Driven Flow
Zone B
Transition between gravity dominated flow and shear driven flow zone
∂1 B: x* ≈ 0
∂2 B: x* ≈ x0.7
∂2 A : x** ≈ x0.7
Zone A
Shear Driven Flow Zone
Correlation presented for this region
∂1 A: x** ≈ 0
Gravity Dominated Flow Zone
Rein
Gp = Fr -1x* Rein 2
10000
9000
8000
7000
6000
5000
4000
3000
2000
1000
0
0
50000
100000
150000
200000
250000
300000
350000
400000

Fig.6d

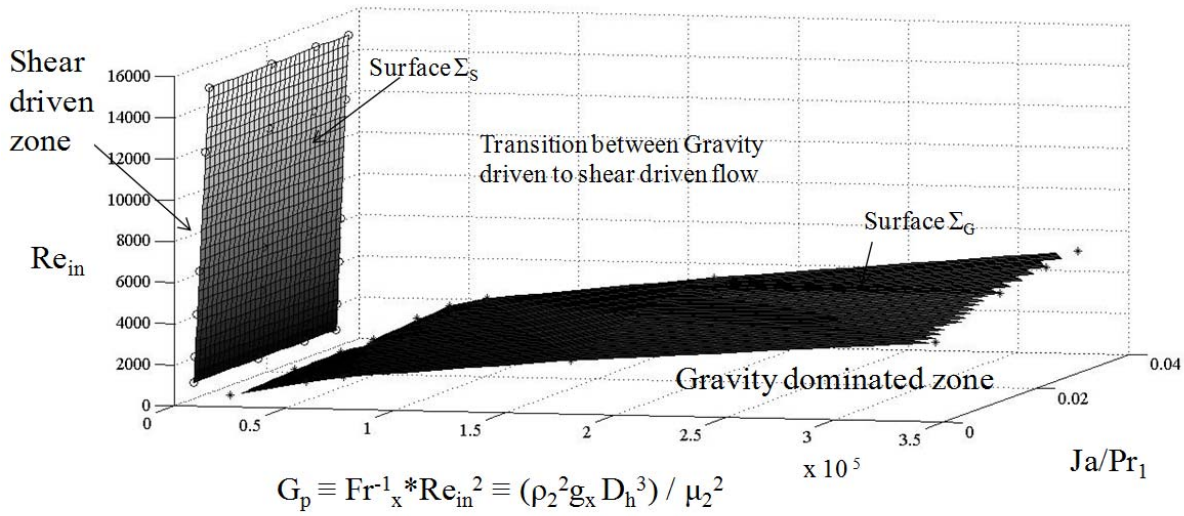
Shear driven zone
Surface Σ_S
Transition between Gravity driven to shear driven flow
Surface Σ_G
Re_{in}
Gravity dominated zone
16000
14000
12000
10000
8000
6000
4000
2000
0
0.5
1
1.5
2
2.5
3
3.5
x 10 5
0.04
0.02
0
Ja/Pr_1
$G_p \equiv Fr^{-1}_x * Re_{in}^2 \equiv (\rho_2^2 g_x D_h^3) / \mu_2^2$

Fig. 7a

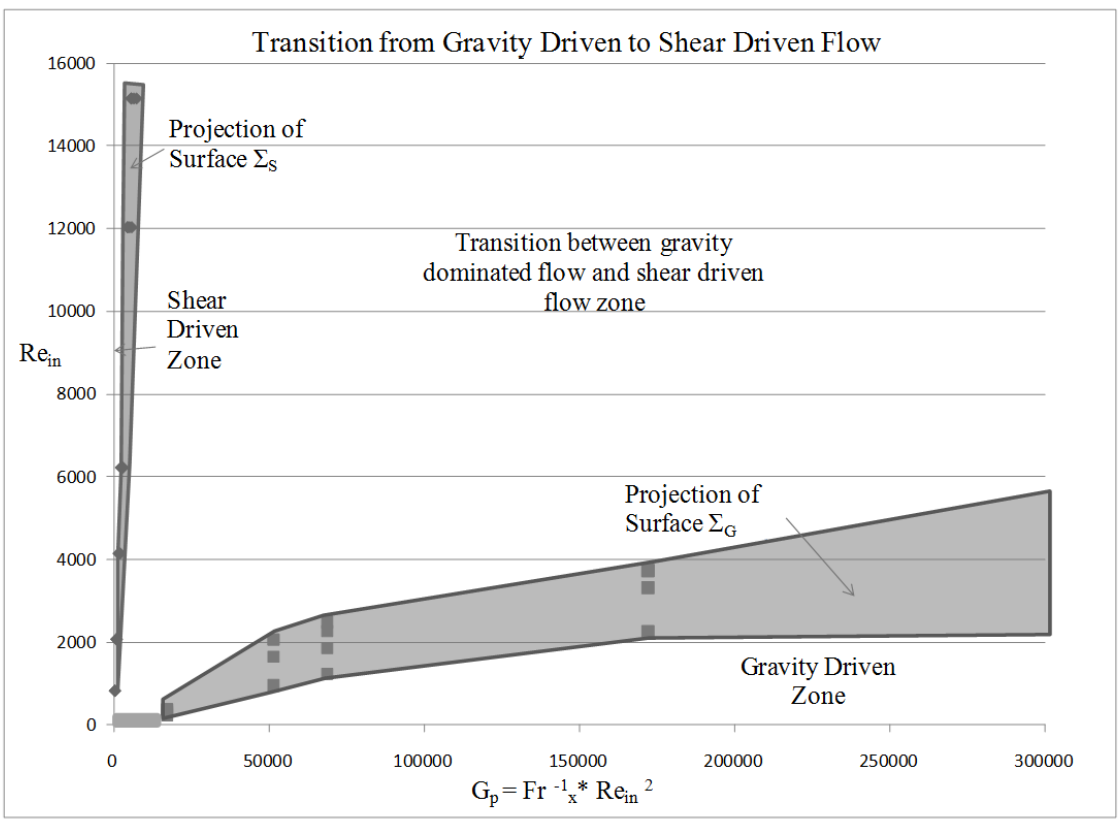
Transition from Gravity Driven to Shear Driven Flow
Projection of Surface Σ_S
Transition between gravity dominated flow and shear driven flow zone
Shear Driven Zone
Re_{in}
Projection of Surface Σ_G
Gravity Driven Zone
16000
14000
12000
10000
8000
6000
4000
2000
0
0
50000
100000
150000
200000
250000
300000
$G_p = Fr^{-1}_x * Re_{in}^2$

Fig. 7b

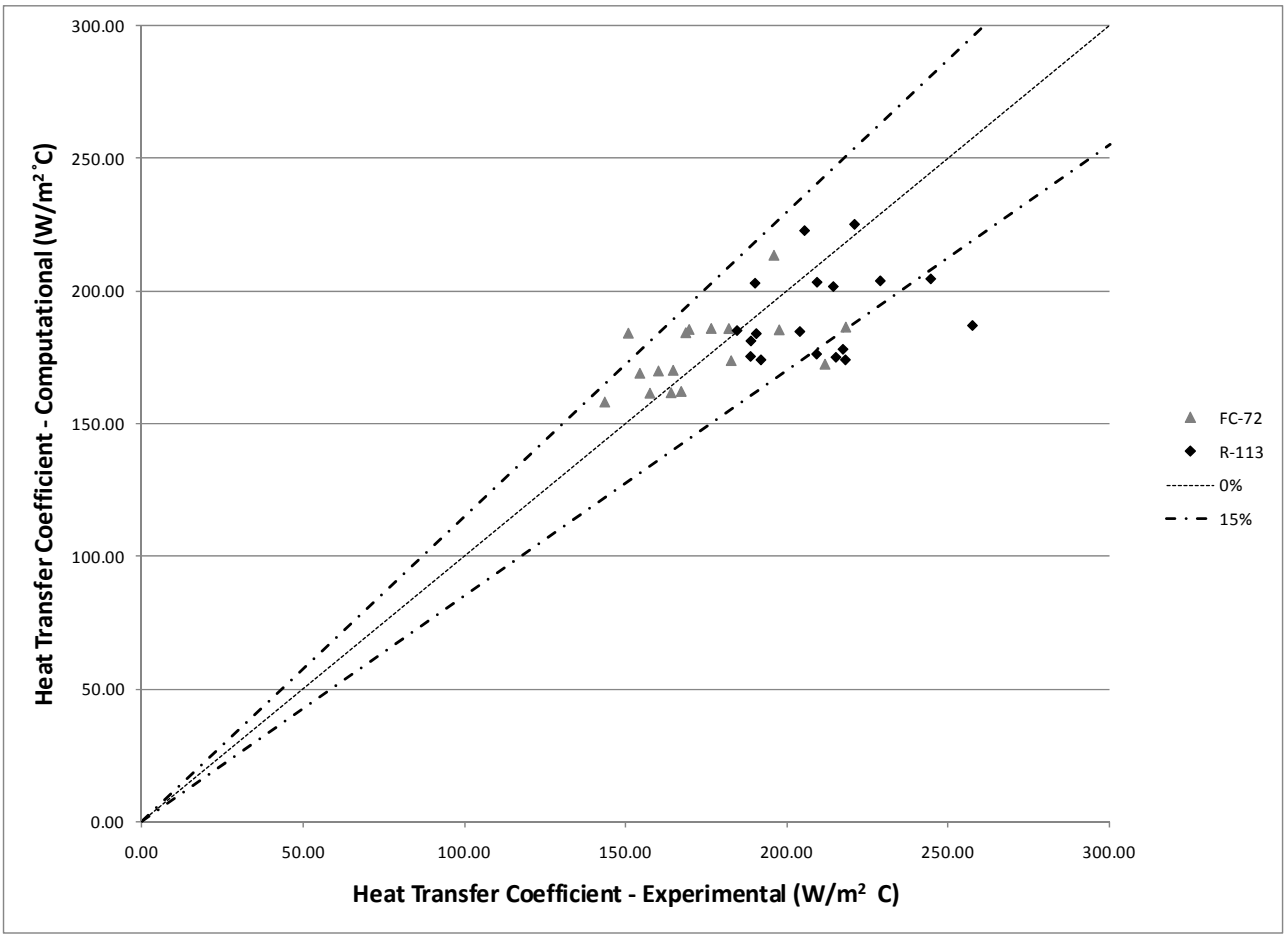
300.00
250.00
200.00
150.00
100.00
50.00
0.00
0.00
50.00
100.00
150.00
200.00
250.00
300.00
Heat Transfer Coefficient - Computational (W/m² °C)
Heat Transfer Coefficient - Experimental (W/m² C)
FC-72
R-113
0%
15%

Fig. 8

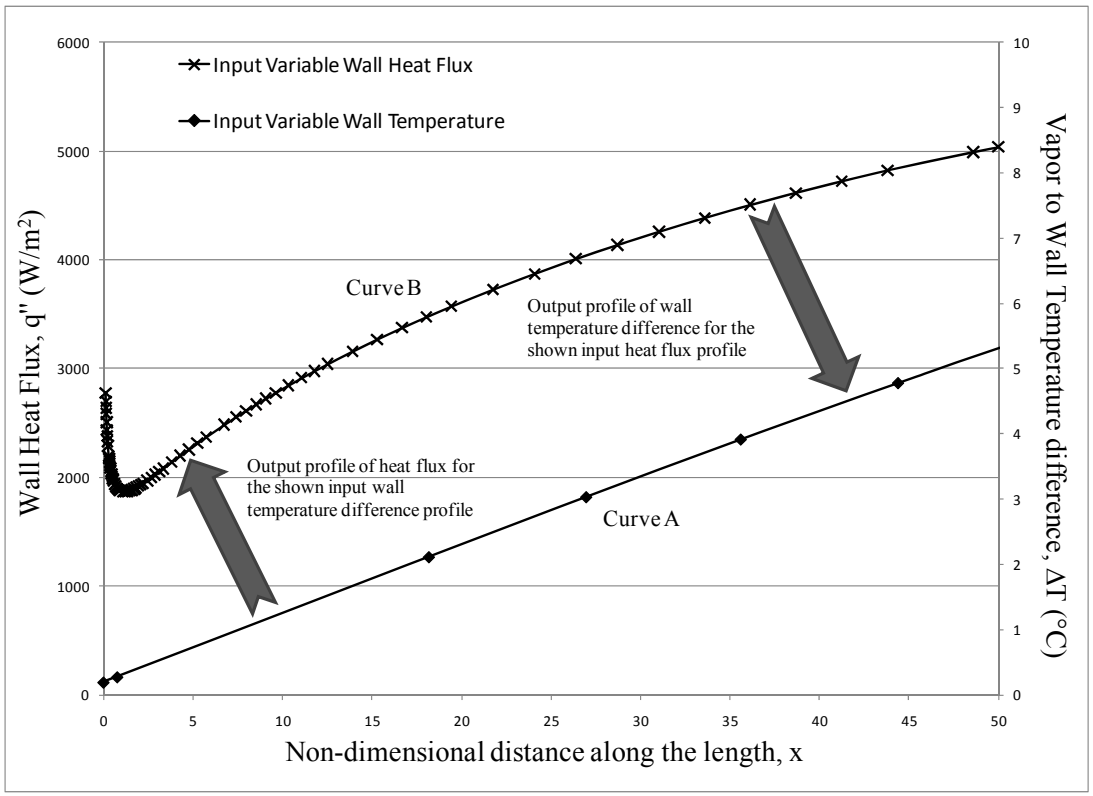
Input Variable Wall Heat Flux
Input Variable Wall Temperature
Wall Heat Flux, q" (W/m2)
Vapor to Wall Temperature difference, ΔT (°C)
Non-dimensional distance along the length, x
Curve B
Curve A
Output profile of wall temperature difference for the shown input heat flux profile
Output profile of heat flux for the shown input wall temperature difference profile
0
1000
2000
3000
4000
5000
6000
0
1
2
3
4
5
6
7
8
9
10
0
5
10
15
20
25
30
35
40
45
50

Fig. 9a

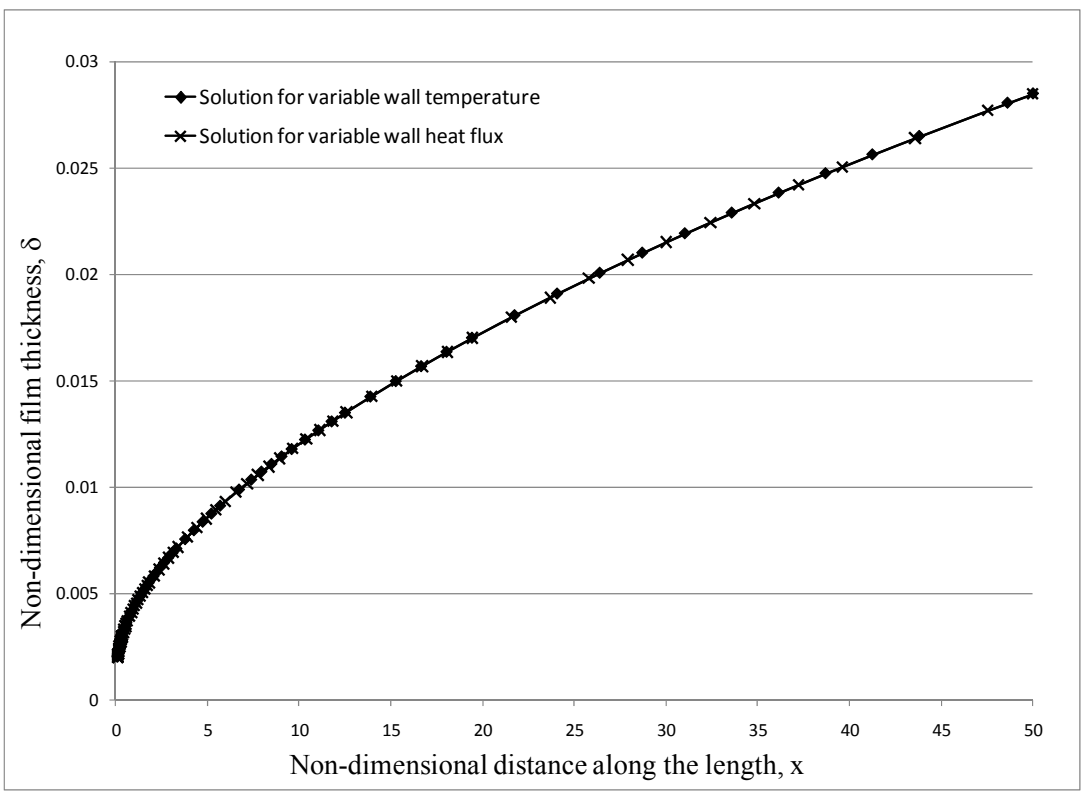
Solution for variable wall temperature
Solution for variable wall heat flux
Non-dimensional film thickness, δ
Non-dimensional distance along the length, x
0
0.005
0.01
0.015
0.02
0.025
0.03
0
5
10
15
20
25
30
35
40
45
50

Fig. 9b

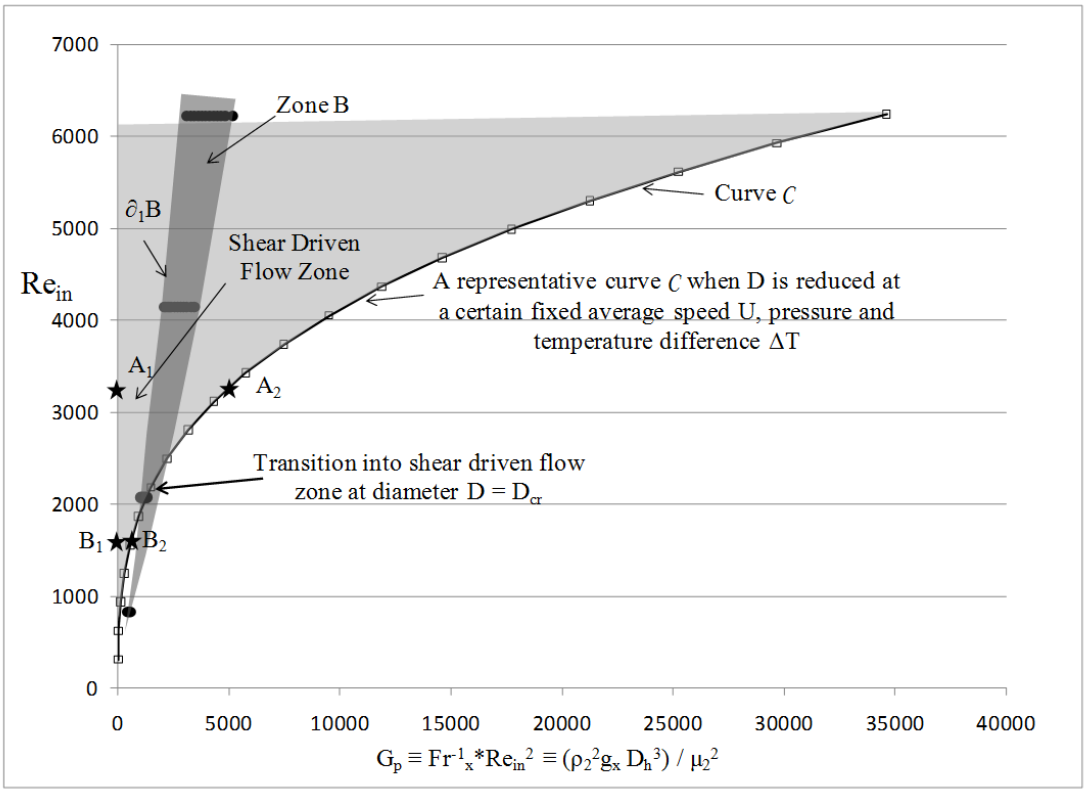

Fig. 10a

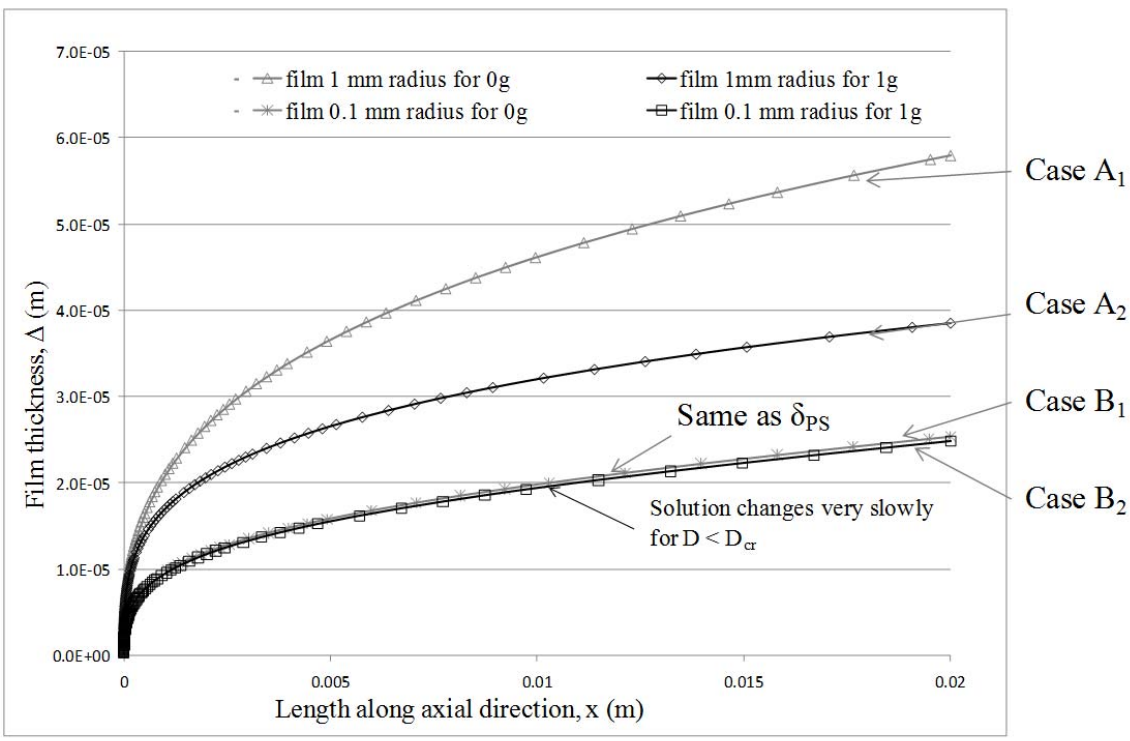

Fig. 10b

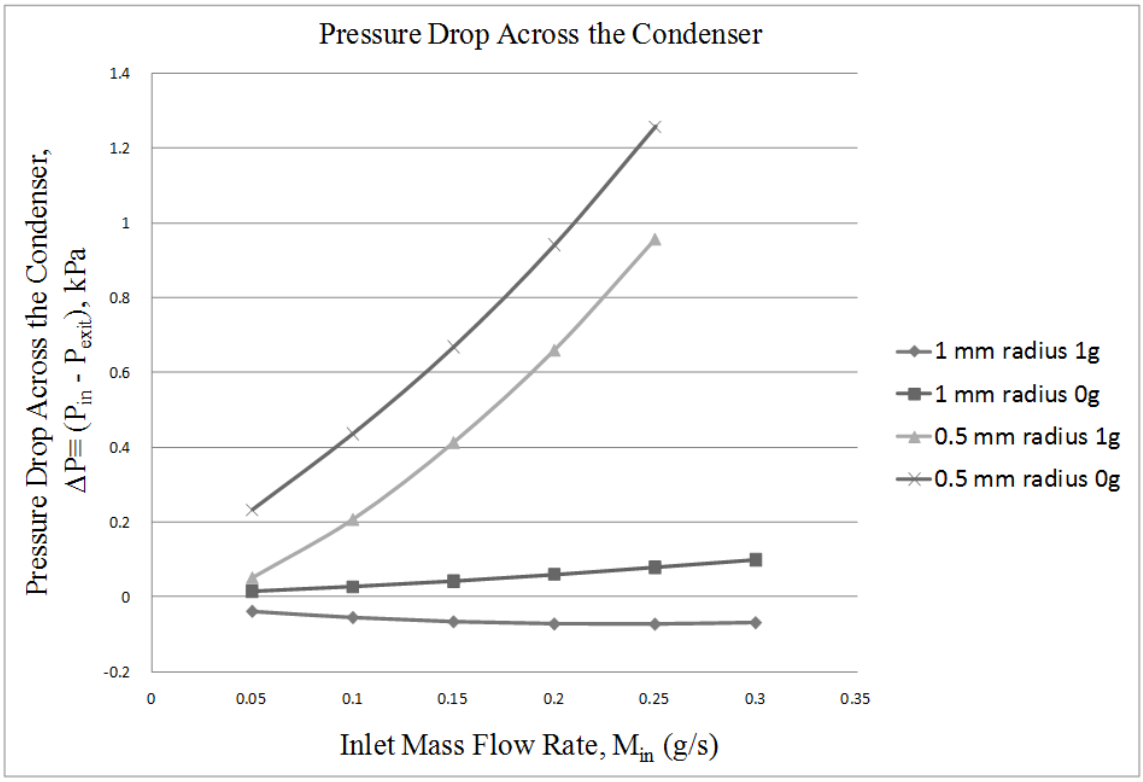
Pressure Drop Across the Condenser
Pressure Drop Across the Condenser, ΔP≡ (P_in - P_exit), kPa
1.4
1.2
1
0.8
0.6
0.4
0.2
0
-0.2
0
0.05
0.1
0.15
0.2
0.25
0.3
0.35
Inlet Mass Flow Rate, M_in (g/s)
1 mm radius 1g
1 mm radius 0g
0.5 mm radius 1g
0.5 mm radius 0g

Fig. 10c

Table Captions:

Table 1: Comparison of experimental results of Lu and Suryanarayana for FC-72 vapor with computationally obtained results for an inclined channel with 1° inclination. The values of $h_t \equiv \dot{Q} / (A.\Delta T)$, where $\dot{Q}$ is total heat removal (in W) for a condensing-surface area of $A = 0.04\ m^2$

Table 2: Comparison of experimental results of Lu and Suryanarayana for R113 vapor with computationally obtained results for an inclined channel with 1° inclination. The values of $h_t \equiv \dot{Q} / (A.\Delta T)$, where $\dot{Q}$ is total heat removal (in W) for a condensing-surface area of $A = 0.04\ m^2$

Tables:

Table 1:

Run	M_{in}	ΔT	Film Thickness - Experimental, (mm) at different x (mm)					Film Thickness - Computational, (mm) at different x (mm)					h_t-exp	h_t-comp	h_t-Nu
	* 10^3 (kg/s)	(°C)	x = 50.8	x = 152.4	x = 254	x = 457.2	x = 812.2	x = 50.8	x = 152.4	x = 254	x = 457.2	x = 812.2	(W/m^2.°C)	(W/m^2.°C)	(W/m^2.°C)
322	4.77	20.26	0.24	0.32	0.34	0.34	0.37	0.19	0.25	0.29	0.33	0.38	150.84	184.12	165.55
317	6.29	30.23	0.27	0.40	0.40	0.41	0.42	0.21	0.27	0.31	0.36	0.42	160.15	169.95	153.04
321	6.73	19.67	0.20	0.31	0.32	0.34	0.36	0.19	0.25	0.28	0.33	0.38	176.47	185.90	166.67
313	7.87	31.37	0.24	0.37	0.41	0.42	0.44	0.21	0.27	0.31	0.36	0.42	154.41	169.09	151.74
320	7.73	19.86	0.19	0.32	0.33	0.34	0.36	0.19	0.25	0.28	0.33	0.38	169.64	185.53	166.23
312	8.15	40.86	0.22	0.40	0.46	0.48	0.51	0.22	0.29	0.33	0.38	0.44	157.52	161.62	145.19
319	9.06	20.47	0.18	0.29	0.32	0.34	0.37	0.19	0.25	0.29	0.33	0.38	168.60	184.31	165.12
331	9.16	10.53	0.17	0.24	0.26	0.27	0.28	0.16	0.22	0.25	0.29	0.33	195.85	213.33	190.52
311	10.89	41.12	0.21	0.36	0.43	0.48	0.50	0.22	0.29	0.33	0.38	0.44	164.07	161.80	145.01
345	11.23	40.58	0.22	0.35	0.42	0.46	0.48	0.22	0.29	0.33	0.38	0.44	167.19	162.29	145.43
314	11.21	30.81	0.23	0.30	0.37	0.40	0.44	0.21	0.27	0.31	0.36	0.42	164.71	170.21	152.32
346	11.64	28.21	0.21	0.30	0.37	0.39	0.40	0.20	0.27	0.30	0.35	0.41	182.64	173.82	155.43
301	12.29	47.58	0.29	0.39	0.39	0.42	0.53	0.22	0.29	0.33	0.39	0.45	143.56	158.31	141.89
323	12.77	20.12	0.17	0.27	0.30	0.32	0.34	0.19	0.25	0.28	0.33	0.38	181.91	185.86	165.85
324	14.57	20.32	0.17	0.28	0.28	0.29	0.34	0.19	0.25	0.29	0.33	0.38	197.49	185.37	165.21
315	15.68	29.88	0.19	0.28	0.33	0.37	0.37	0.20	0.27	0.31	0.36	0.41	211.63	172.48	153.88
325	17.13	19.99	0.20	0.28	0.30	0.31	0.31	0.19	0.25	0.28	0.33	0.38	218.08	186.41	165.83

Table 2:

Run	M_{in}	ΔT	Film Thickness - Experimental, (mm) at different x (mm)					Film Thickness - Computational, (mm) at different x (mm)					h_t-exp	h_t-comp	h_t-Nu
	* 10^3 (kg/s)	(°C)	x = 50.8	x = 152.4	x = 254	x = 457.2	x = 812.2	x = 50.8	x = 152.4	x = 254	x = 457.2	x = 812.2	(W/m^2.°C)	(W/m^2.°C)	(W/m^2.°C)
221	2.45	21.42	0.19	0.32	0.35	0.39	0.44	0.23	0.30	0.35	0.40	0.46	190.18	202.76	181.94
220	2.58	31.21	0.25	0.38	0.40	0.46	0.51	0.26	0.34	0.38	0.45	0.51	184.61	184.93	165.88
100	3.19	14.76	0.31	0.35		0.38	0.38	0.21	0.27	0.31	0.36	0.42	205.50	222.52	199.26
180	4.17	33.83	0.30	0.36	0.41	0.43	0.47	0.26	0.34	0.39	0.45	0.52	188.91	181.03	162.91
181	3.99	21.42	0.19	0.29	0.32	0.34	0.40	0.23	0.30	0.34	0.40	0.46	209.36	203.12	182.05
182	4.37	14.15	0.23	0.26	0.28	0.32	0.36	0.20	0.27	0.31	0.35	0.41	220.96	224.89	201.58
202	5.32	32.19	0.22	0.34	0.41	0.44	0.48	0.26	0.34	0.38	0.45	0.52	190.57	183.77	164.91
201	5.22	39.79	0.26	0.37	0.42	0.44	0.50	0.28	0.36	0.41	0.48	0.56	192.00	173.90	156.23
203	5.29	20.11	0.17	0.28	0.31	0.34	0.41	0.28	0.36	0.41	0.48	0.56	218.14	173.90	184.67
225	5.45	38.71	0.24	0.38	0.44	0.47	0.52	0.27	0.36	0.41	0.48	0.55	188.79	175.19	157.19
207	6.6	31.62	0.18	0.29	0.34	0.40	0.43	0.26	0.34	0.39	0.45	0.52	204.04	184.56	165.37
208	6.82	22.28	0.15	0.30	0.34	0.37	0.40	0.23	0.31	0.35	0.40	0.47	214.40	201.49	180.22
195	7.42	38.28	0.18	0.32	0.37	0.42	0.47	0.27	0.36	0.41	0.47	0.55	209.23	176.08	157.68
211	8.43	21.20	0.13	0.27	0.30	0.37	0.40	0.23	0.30	0.34	0.40	0.46	244.53	204.37	182.32
223	9.51	37.03	0.17	0.29	0.36	0.42	0.50	0.27	0.35	0.40	0.47	0.54	217.38	177.88	159.03
213	9.86	39.73	0.15	0.30	0.37	0.44	0.53	0.27	0.36	0.41	0.48	0.55	215.20	174.88	156.36
215	9.76	21.65	0.11	0.20	0.25	0.35	0.38	0.23	0.30	0.35	0.40	0.46	228.93	203.61	181.36
206	13.21	30.95	0.17	0.28	0.34	0.38	0.41	0.25	0.33	0.38	0.44	0.51	257.44	186.82	166.26